Alleviating Hypoxia Through Self-Generating Oxygen and Hydrogen Peroxide Fluorinated Chitosan: insights from a kinetic study

Pejman Ghaffari-Bohlouli[a], *Houman Alimoradi*[a], *Denise Freitas Siqueira Petri*[b], *Saeid Moghassemi*[c], *Christiani A. Amorim*[c], *Lei Nie*[d], *Amin Shavandi*[a*]

[a] *Université libre de Bruxelles (ULB), École polytechnique de Bruxelles, 3BIO-BioMatter lab, Avenue F.D. Roosevelt, 50 - CP 165/61, 1050 Brussels, Belgium*

[b] *Fundamental Chemistry Department, Institute of Chemistry, University of São Paulo,* Av. *Prof. Lineu Prestes 748, São Paulo, 05508-000, Brazil*

[c] *Pôle de Recherche en Physiopathologie de la Reproduction, Institut de Recherche Expérimentale et Clinique, Université Catholique de Louvain, Brussels, Belgium*

[d] *College of Life Sciences, Xinyang Normal University, Xinyang 464000, China*

* Corresponding author: Email: amin.shavandi@ulb.be, Tel: +326503681

Abstract

Effective methods to alleviate hypoxia are necessary for the proper healing of chronic wounds. However, current oxygen (O_2) delivery methods suffer from limitations, such as low O_2 capacity and short supply time, burst release, and inadequate O_2 preservation potential. This study presents a new approach utilising fluorinated chitosan (PFC-chitosan) infused with self-generating and preserving O_2 and hydrogen peroxide (H_2O_2). We incorporated calcium peroxide (CaO_2)-loaded polycaprolactone (PCL) particles into the PFC-chitosan matrix and subsequently evaluated the release kinetics of O_2 and H_2O_2 from these materials. The incorporation of CaO_2 into PCL particles and PFC-chitosan effectively mitigate the rapid decomposition rate of CaO_2 while the PFC groups enable the dissolution of generated O_2 via Van der Waals interactions. The apparent rate constant (k_{O_2}) for O_2 release from CaO_2 under hypoxia decreased from 1.194 μM^{-1} h^{-1} to 0.141 μM^{-1} h^{-1} by incorporating into PCL particles and PFC-chitosan, indicating the slower release of O_2 from these materials. Regarding release kinetics, H_2O_2 follows a pseudo-zero-order pattern, while O_2 exhibits a pseudo-first-order pattern. The k_{O_2} is affected by temperature, pH, initial O_2 concentration in the release media, and an initial amount of CaO_2. The particles with PFC-chitosan showed higher cell viability and slower O_2 release rates, indicating improved angiogenesis potential. The simultaneous generation of O_2 and H_2O_2 from PFC-chitosan may have the potential to improve chronic wound healing by providing a continuous supplying of O_2.

Keywords: alleviating hypoxia, inducing oxidative stress, oxygen generating, hydrogen peroxide generating, fluorinated chitosan, wound dressing

1. Introduction

The healing process for chronic wounds can take several months if the inflammation phase is not successfully passed[1]. In chronic wounds, hypoxia, insufficient tissue oxygenation (O_2 concentration is 5% or lower), hinders epithelization, angiogenesis, and collagen deposition, resulting in a slower healing process[1]. Exogenous oxygenation of the wounds during the healing process could affect signaling molecules, including cytokines, matrix metalloproteinases (MMPs), growth factors, and proteases, therefore, accelerating wound healing[2].

Various approaches have been applied to provide O_2 to hypoxic tissues, such as hyperbaric oxygenation, utilizing O_2-carriers, and O_2-generating biomaterials[3]. Hyperbaric O_2 therapy (HBOT) has been proven effective in treating chronic wounds through multiple clinical trials. However, it is important to carefully assess and monitor the potential complications of HBOT, including barotraumatic lesions, O_2 toxicity, and confinement anxiety. Additionally, the cost of the necessary equipment and the risk of using high-pressure capsules are limitations of HBOT[4, 5].

O_2-generating biomaterials such as peroxides, nanozymes, MnO_2-based particles, and algae can show a wide range of release from several hours to even more than a month. This release time is determined by the physicochemical properties of the biomaterial, the condition in which it is released, and methods used for delivery and prevent of rapid release[3]. Nanozymes and MnO_2-based particles, although incapable of generating O_2 independently, play a vital role in the presence of H_2O_2 for O_2 production[3]. As a result, these materials possess the ability to alleviate oxidative stress while simultaneously generating O_2 within tumor tissues[3]. Conversely, the strategy of utilizing algae to produce O_2 relies on the use of living xenogeneic matter, which can potentially lead to immune incompatibility and cytotoxicity[6]. An alternative approach for achieving a maximal O_2 payload and a more gradual release of O_2 involves the utilization of solid peroxides.

Due to less water solubility and higher purity compared with most peroxides, CaO_2 has been introduced as an ideal O_2-generating source for biomedical applications[7]. The CaO_2 dissolution rate in water and the resulting O_2 generation can be extended by incorporating it into hydrophobic shells. However, preventing the burst O_2-release and low O_2 preservation in such structures remain the main challenge[7]. At high O_2 concentrations, the excess of univalent

reduction of O_2, which generates reactive O_2 species (ROS), overwhelms the natural antioxidant defense system and results in cellular toxicity[8].

O_2 carrier materials such as hemoglobin (Hb), transfused red blood cells (RBC), and perfluorocarbons (PFCs), were proposed as an alternative approach for the delivery of O_2 to the hypoxic tissues[3]. PFCs are hydrophobic molecules with O_2 dissolving capacity approximately 20 times greater than water. The Food and Drug Administration (FDA) has approved the use of some PFCs in humans due to their proven safety and effectiveness in supplying O_2[9]. However, the existing PFC-based O_2 carriers have limited O_2 payload capacity, resulting in a short-time O_2 supply, a burst O_2 release profile, and hydrophobic properties, hindering their effectiveness for wound healing applications[3]. Thus, to deliver O_2, PFCs need to be loaded in an environment that is saturated with O_2. To improve the hydrophobicity of PFCs for more efficient and localized O_2 delivery in diabetic wounds, PFCs were conjugated with methacrylamide chitosan[10]. The resulting hydrogels were able to supply O_2 for up to only 12h[10].

So far, polycaprolactone (PCL), poly lactic acid (PLA), poly(lactide-co-glycolide) (PLGA), polyurethane (PU), poly(N-vinylpyrrolidone) (PVP), and N-isopropyl acrylamide have been used as a hydrophobic cover to prolong O_2 release from CaO_2 by blocking the accessibility of water to CaO_2[3]. Mohseni-Vadeghani et al. used PLA as a hydrophobic shell to prevent the fast degradation of CaO_2. In this study, the highest concentration of O_2 was observed during the first days[11]. Although the extension of O_2 release from CaO_2 has been achieved through its encapsulation into various polymers with diverse structures, the initial burst release and low O_2 preservation in the release media remain challenging[12-16].

Skin wounds can have different pH[17] and temperature[18] which can affect the kinetic and yield of O_2 and H_2O_2 from CaO_2. While Wang *et al*. studied the kinetic of the produced O_2 and H_2O_2 resulting from pure CaO_2 decomposition under varying temperatures and pH levels[19] there is no study on the kinetic of O_2 and H_2O_2 generated from biomaterials such as encapsulated CaO_2 into a hydrophobic polymer to investigate the effect of the coating on the release rate of O_2 and H_2O_2 under various conditions that a wound can have.

The objective of this study was to develop a catalytic biomaterial to achieve sustained release and preservation of O_2. We combined O_2-generating peroxides with PFC O_2-carriers to design a self O_2 generating carrier biomaterials without the need for reloading. To prevent the rapid release

of O_2 and H_2O_2, we coated CaO_2 particles with PCL and doped them with PFC-conjugated chitosan. We hypothesized that the PFCs groups on chitosan can control the release of O_2 from the PCL particles and release the trapped O_2 in a sustained manner. This combination served as protective and O_2-buffering shells, enabling the release of O_2 in a controlled manner through catalase-catalyzed decomposition of H_2O_2. The kinetic of generated O_2 and H_2O_2 from the covered CaO_2 was calculated to study the effect of different release conditions such as initial O_2 concentration of release media (hypoxia and normoxia), the amount of incorporated CaO_2, the volume of release media, pH and temperature of release media, and catalase on O_2 and H_2O_2 release.

In the present work, the PCL particles extended the termination time of CaO_2 decomposition. The findings demonstrate that PFCs can adsorb O_2 generated by CaO_2 and supply it at a gradual rate, thereby preventing any depletion in the concentration of O_2 following rapid release. Furthermore, the presence of PFC groups was found to impede the initial burst release, which could potentially reduce any cytotoxicity associated with the burst release of O_2. Therefore, the utilization of PFC-chitosan not only exhibited the ability to decelerate the initial burst release of O_2 from the PCL particles but also extended the supply of O_2 in the release media.

2. Materials and methods

2.1 Synthesis of the CaO_2-loaded PCL particles

The CaO_2-loaded PCL particles were synthesized by incorporating CaO_2 as the hydrophilic phase into polycaprolactone (PCL, average M_n=80000, $M_wM_n^{-1}$ <2, Sigma-Aldrich) as the hydrophobic phase[20, 21]. Known amounts of CaO_2 (white powder with a purity of 75%, Sigma-Aldrich) (0, 0.1, 0.25, 0.5, and 1.0% (wt v^{-1})) were suspended in a 10% (wt v^{-1}) solution of PCL in dichloromethane (DCM, Thermo fisher scientific) and named PX, which X is the content of CaO_2 (Table 1).

Then, the suspensions were sonicated for 10 minutes and added to 2% (wt v^{-1}) of homogenized polyvinyl alcohol (PVA, M_w=9000-10000 kDa, 80% hydrolyzed, Sigma-Aldrich) solution in deionized (DI) water at 1:20 (v:v). The synthesized CaO_2-loaded PCL particles containing CaO_2 were precipitated via centrifugation at 104 RCF for 1 minute to collect the precipitated particles and the supernatant was quickly decanted to minimize the decomposition of the loaded CaO_2 during the synthesis. To ensure the separation of PVA from the surface of the

synthesized particles, the CaO_2-loaded particles were washed with DI water and precipitated by centrifugation several times, and then, freeze-dried.

2.2 Synthesis of the PFC-chitosan film

Pentadecafluorooctanoyl chloride (PFC, 97%, M_w of 432.51 Da, Merck) was conjugated on chitosan (M_w of 50-190 kDa, DD ≥ 75%, Biosynth-Carbosynth) as was reported before with slight modifications[22-24]. Briefly, 1.85 mmol of the chitosan was dissolved in DI water: tetrahydrofuran (THF) (1:1, v:v) containing 2% (v v^{-1}) acetic acid to reach a 3% wt v^{-1} of chitosan solution. Then 1.40 mmol of the PFCs were added into the solution dropwise and stirred at 100 rpm for 24 hours at ambient temperature. The reaction mixture was purified via a dialysis bag (3500 Da, in which the cutoff was larger than PFC molecules) against distilled water for three days with three daily changes, then lyophilized.

2.3 PFC-chitosan films loaded with CaO_2- PCL particles

The synthesized PFC-chitosan was dissolved in THF/DI water (50:50 v v^{-1}) containing 2% (v v^{-1}) acetic acid so that the concentration of PFC-chitosan solution reached 2% (wt v^{-1}), then various ratios of P1 particles were incorporated into the PFC-chitosan solution (0:1, 0.5:1, and 1:1 (particles: film (wt wt^{-1})), which named P1F0, P1F0.5, and P1F1 (Table 1), and then sonicated for 5 minutes to disperse the particles. The homogenized solutions were cast into a silicon mold and dried under a vacuum at 30 °C.

Table 1. Composition of the synthesized particles and PFC-chitosan films loaded with particles.

Sample		CaO_2 concentration (%)	Ratio between PCL particles and PFC-chitosan ((particles: film) wt wt^{-1})
Particles	P0	0	-
	P0.1	1	-
	P0.25	2.5	-
	P0.5	5	-
	P1	10	-
Films	P1F0	10	0:1
	P1F0.5	10	0.5:1
	P1F1	10	1:1

2.4 Experimental procedures to study the kinetics of generated O_2 and H_2O_2

For kinetics studies, a known amount of the particles and films containing 15 mg of CaO_2 were dispersed into the release media (DI water). A 100 mL cylindrical plastic reactor with the ability to maintain the inside pressure constant was used for the kinetic studies.

We evaluated the effect of pH, temperature, and concentration of initial O_2 of the released media on the kinetics and release of O_2 and H_2O_2. Hypoxia condition (initial O_2 concentration $\leq$ 5%) was achieved by purging the release media with nitrogen (N_2) for 20 minutes. The pH of the medium was adjusted with 1.0 M HCl or 1.0 M NaOH. To prevent the unwanted decomposition of the generated H_2O_2 to O_2 by light and temperature, the reactor was wrapped with aluminum foil and incubated in an incubator. All of the experiments were conducted in triplicate.

2.4.1 O_2 and H_2O_2 release in normoxia and hypoxia

The release of O_2 and H_2O_2 from CaO_2 and P1 particles was investigated under normoxia and hypoxia at pH 7.4, and room temperature. 15 mg of CaO_2 and a certain amount of P1 particles containing 15 mg of CaO_2 were added into 50 mL of the release media in the reactor. The gas and solution phases were monitored separately for O_2 using a contactless sensor (PreSens, Regensburg, Germany)[25, 26]. In contrast, the H_2O_2 release was measured in the solution phase using Pierce quantitative peroxide assay kits (Thermos Scientific Pierce, Rockford, IL, USA), as previously reported[25]. Figure 1 represents the measuring procedure of O_2 and H_2O_2.

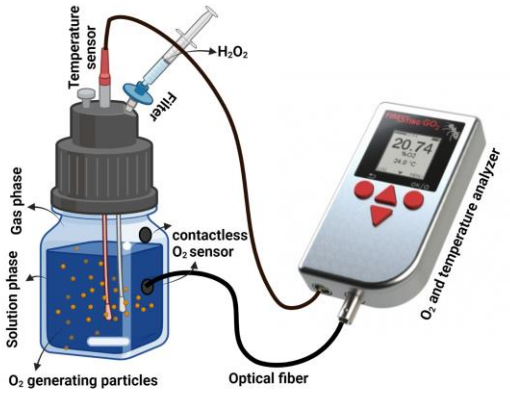

Figure 1. Experimental procedure to determine the amount of O_2 in the gas and solution phases and of H_2O_2 in the solution phase.

2.4.2 Effect of the media volume on the release of O_2 and H_2O_2

We studied the potential effect of the media volume on the release of O_2 and H_2O_2. For this experiment, 15 mg of CaO_2 and a specific amount of P1 particles containing 15 mg of CaO_2 were dispersed into varying volumes of the release media (25 mL (0.6 mg mL^{-1}), 50 mL (0.3 mg mL^{-1}), and 100 mL (0.15 mg mL^{-1})). The pH (7.4), room temperature, and initial O_2 concentration (≤5%) were kept constant.

2.4.3 Effect of the initial amount of CaO_2 on the release of O_2 and H_2O_2

To investigate the effect of the initial amount of CaO_2 on the release of O_2 and H_2O_2, 5, 15, and 25 mg of CaO_2 and a certain amount of P1 particles containing 5 (0.05 mg mL^{-1}), 15 (0.15 mg mL^{-1}), and 25 mg (0.25 mg mL^{-1}) of CaO_2 were added to 100 mL of release media with an initial O_2 concentration ≤ 5%, at room temperature, and pH of 7.4.

2.5 Characterization of the particles and the PFC-chitosan films

2.5.1 Proton, Fluorine-19 nuclear magnetic resonance (^1H NMR and ^{19}F NMR) and Fourier Transform Infrared Spectroscopy (FTIR)

High-resolution ^{19}F and ^1H NMR experiments were recorded on a 400 MHz Varian INOVA spectrometer to investigate the conjugation of the PFC groups on the chitosan. The synthesized PFC-chitosan was dissolved into a solution of deuterated THF/DI water/acetic acid (49:49:2V/V%). To determine the substitution degree of the PFC groups on the chitosan, the integration of the corresponding peak between -125 to -79 ppm areas in ^{19}F NMR was calculated using the trichlorofluoromethane's peak as the reference[23]. The substitution degree was calculated using Equation 1:

$$DF = \sum \left(1 + \left\{ \frac{\frac{I_{CFn}}{I_{ref}}}{m_f} \right\} \right) \times 100 \quad (1)$$

Where DF is the degree of fluorination, I_{CFn} and I_{ref} is the integral intensity related to each fluorine peak area and reference CF groups, respectively, in ^{19}F NMR. m represents the number of fluorine in the related peak.

The infrared spectra of the chitosan and the PFC-chitosan were obtained using an ATR-FTIR-6600 spectrometer (JASCO, Japan) with a resolution of 4 cm^{-1} and 32 scans per spectrum.

2.5.2 *Morphological properties*

The morphology of the CaO_2-loaded PCL particles with various concentrations of CaO_2 and the cross-section of the PFC-chitosan film containing P1 particles were investigated using an optical microscope and scanning electron microscopy (SEM, HITACHI, SU-70, Japan). To calculate the average diameter of the particles, the SEM images were analyzed using ImageJ software. The measurements were carried out in triplicate and 50 particles were measured for every sample. The surface roughness and topography of the thin films with a thickness of ~ 100 µm were studied by AFM on a Multimode 8 (Bruker, Germany). The AFM was carried out in tapping mode, with a resolution of 512 pixels and a force constant cantilever of 42 N m^{-1}, and in the air[27].

Brunauer-Emmett-Teller (BET) analysis was performed to determine the size of porosities and specific surface areas of the particles which were used for O_2 and H_2O_2 release and kinetic studies [28]. The N_2 adsorption/desorption isotherm was measured using a Micromeritics instrument (crop., Norcross GA, USA, ASAP 2020). Before the analysis, the particles were degassed at 40 °C for 6 hours.

2.5.3 *Amount of CaO_2 loaded its encapsulation efficiency*

The encapsulation efficiency and loading content of CaO_2 in the PCL particles were examined by dissolving the PCL shell[20]. To dissolve the PCL shell of the particles, 500 mg of the CaO_2-loaded PCL particles were dispersed in 10 mL of DCM for 4 hours at room temperature. The CaO_2 was then separated by centrifugation at 5000 RCF for 5 minutes. To dissolve PCL and separate the CaO_2, the procedure was repeated three times. The dried weight of the separated CaO_2 was measured to calculate the encapsulation efficiency and loading content according to Equations (2) and (3):

$$\text{Encapsulation efficiency} = \frac{\text{Dried weight of the separated } CaO_2\ (mg)}{\text{Weight of initial } CaO_2 \text{ in the synthesizing solution (mg)}} \times 100 \quad (2)$$

$$CaO_2 \text{ Loading content} = \frac{\text{Dried weight of the separated } CaO_2 (mg)}{\text{Weight of the initial particles (mg)}} \times 100 \quad (3)$$

2.5.4 *The distribution of the incorporated CaO_2 into the PCL particles*

To measure the distribution of the incorporated CaO_2 into the PCL particles alizarin red staining was used[11]. 30 mg of the PCL particles loaded with CaO_2 and plain PCL particles were incubated with 2% wt v^{-1} alizarin red (product number D0242 and purity ≥ 95%, TCI). The pH of

the solution was adjusted to 4.2 using 0.5% v v^{-1} ammonia hydroxide and the incubation was carried out at room temperature for 4 hours. Then the stained particles were washed three times with DI water and precipitated by centrifugation (104 RCF for 1 min). The stained particles were observed by an inverted fluorescence microscope with a bandpass filter with a wavenumber of 530-580 nm and a 20X objective[20].

2.5.5 Water contact angle (WCA), swelling, and degradation of the films

The surface and bulk hydrophilicity of the films were evaluated based on the sessile drop method and the water uptake capacity method[29]. A G10 contact goniometer (SEO Phoenix, Korea) was used to measure the wettability of the surface of the films by dispensing 8 μL of DI droplets. An average of 5 WCA examinations after 10 seconds was reported for each sample at room temperature[29]. The water uptake capacity and hydrolytic degradation of the films were carried out based on weight changes[29]. The dried films with the initial weight (W_i =100mg) were soaked in 100 mL of the phosphate buffer solution (PBS, pH of 7.4, at 37°C) for 100 hours. At specific time points, the samples were taken out and weighted (W_t) after absorbing the excess surface water with a filtering paper. The swelling ratio was calculated based on Equation (4):

$$\text{Water uptake} = \frac{(W_t - W_i)}{W_i} \times 100 \quad (4)$$

The weighted dried films (Wi) were immersed into 100 mL of the PBS containing 1000 U/mL lysozyme (pH of 7.4 and temperature of 37 °C)[30]. At predetermined time intervals, the films were removed and dried in an oven at 40 °C for 2 days (W_t). Every 4 days the media were replaced with fresh media. According to Equation 5, the degradation percentage of the films was calculated.

$$\text{Hydrolytic degradation} = (1 - \frac{W_t}{W_i}) \times 100 \quad (5)$$

2.6 In vitro evaluation of the films and particles under hypoxia and normoxia

2.6.1 Cell culture

The fibroblast cells(3T3-L1) were cultured in Dulbecco's modified Eagle's medium (DMEM)/GlutaMAXTM (Gibco, Paisely, UK) supplemented with 10% heat-inactivated fetal bovine serum (HI FBS; 16140071; Gibco, Paisely, UK) and 1% antibiotics and antimycotic (AA) (Gibco, Green Island, NY, USA). After achieving ~90% confluency, cells were cultured in 96-

well plates (4×10^4 cells/well) for in vitro tests. After 2- and 4-days incubation with normoxia or hypoxia conditions, the cytotoxicity of P0, P1, P1F0, P1F0.5, and P1F1 with and without catalase were analyzed.

2.6.2 Cell cytotoxicity measurements with PrestoBlue assay

The PrestoBlueTM HS (Invitrogen, Merelbeke, Belgium) metabolic assay was used to determine the cytotoxicity of the treatment on days 2 and 4[31]. Briefly, after 60 minutes of cell incubation with PrestoBlueTM reagent: cell culture media (1:10 v/v), the cell viability was measured by fluorescence spectroscopy (Multilabel reader, Victor X4, Singapore) at an excitation wavelength of 560 nm and an emission wavelength of 620 nm.

2.6.3 Cell viability measurements with LIVE/DEAD® assay

To measure the viability of the cells the LIVE/DEAD^{TM} Viability/Cytotoxicity kit (Invitrogen, Merelbeke, Belgium) which contains calcein-AM dye and ethidium homodimer-1 to identify live (green) and dead (red) cells, respectively were used.

Cells were treated for 30 minutes at 37 °C in the dark by incubating in DPBS containing 2 mM calcein-AM and 5 mM ethidium homodimer-I. Using inverted fluorescence microscopy (Leica DMIL, Germany), red fluorescence in dead cells was seen at ex/em 495/635 nm, while green fluorescence in living cells was seen at ex/em 495/515 nm[31].

2.6.4 Investigating the intracellular reactive oxygen species (ROS) generation

Fibroblast cells were cultured in a poly-D-lysin (PDL)-coated glass-bottom 96-well plate (MatTek, USA) with a cell density of 5000 cells/well for 24 h. The cells were treated by P0, P1, P1F0, P1F0.5, and P1F1 with and without catalase and after 24 and 48 hours of incubation, the 2,7-Dichlorofluorescein diacetate (DCFH-DA; D6883, Sigma) was used to assess the intracellular ROS generation[32]. Briefly, following a PBS wash, 20 µM DCFH-DA was applied to the cells. After 30 min, the intracellular ROS production was examined using super-resolution 3D microscopy (CX-A Imaging Platform; Nanolive, Tolochenaz, Switzerland). Finally, the intracellular ROS generation was quantified using ImageJ software (version 1.53e, Wayne Rasband, NIH, USA) by measuring the average intracellular fluorescence intensities[33].

2.6.5 Chorioallantoic membrane (CAM) assay

To evaluate the cytocompatibility and angiogenic properties of the developed materials the Chorioallantoic Membrane (CAM) assay was used. The fertilized chicken eggs (Flock Dyuan) were purchased from Vervaeke-Belavi (Tielt, Belgium). The CAM assay was carried out following previously established methods with slight modifications [34, 35] and the control sample was from our previously published study [36]. The eggs were incubated for 72 hours at 37°C in a 75% humidified atmosphere and rotated every 12 hours. The PFC-chitosan films with and without P1 particles were placed on the main vessel junction near the embryo, and the eggs were monitored for 24 and 48 hours. Finally, the CAMs were photographed and analyzed using AngioTool and ImageJ® to quantify the total vessel length and the number of junctions.

2.7 Statistical analysis

All the experiments were carried out in triplicates and were reported as means ± standard deviation (SD). Statistical analysis (Two-way ANOVA) was carried out using GraphPad Prism8 (GraphPad Software Inc., Boston, MA, USA) and the differences were considered significant if $p < 0.05$.

3. Results and discussion

3.1 Characterization of the CaO_2-loaded PCL particles

The PCL particles exhibited a spherical shape and displayed a size distribution ranging from ~2 to 40 μm (Figure 2a and 2b), along with surface porosities at the nanoscale (Figure 2, c1-2). The BET surface area of 0.155 m^2/g, adsorption average pore diameter of 10.77 nm, and desorption average pore diameter of 3.9 nm were obtained for the particle porosities. These values are consistent with the nanometer-scale porosity observed, which is in line with gas adsorption methods' accuracy for pore sizes below 300 nm[37]. However, the SEM images showed the presence of relatively larger pores, ranging from 20 to 600 nm (Figure 2, c1-2) which can be attributed to the evaporation of the hydrophobic phase (DCM) and the decomposition of CaO_2[11, 20]. This discrepancy between the SEM images showing larger pores and the BET analysis showing smaller nanoscale pores can be attributed to the differences in the techniques' sensitivities and the specific characteristics they capture. SEM provides a surface view of the particles, allowing us to observe the larger pores on the outer surface. On the other hand, BET analysis investigates the particle's internal porosity, revealing the fine pores within the particles which are likely to

contribute to the overall surface area of the particles. It is essential to consider that gas release is a complex process influenced by several factors, including the size and distribution of pores and the nature of the encapsulated material. Therefore, the presence of both larger and nanoscale pores in the PCL particles may play a significant role in regulating the release kinetics of O_2 from the encapsulated CaO_2. This observation is one of the limitations of our study and further studies are required to elucidate the exact mechanisms governing gas release and the relationship between the particle porosity and release kinetics.

The average diameter of the particles was measured to be 12.0±0.3 μm, which aligns with a previous study where PCL particles containing CaO_2, produced using the same methodology, had a reported diameter of 11.7 μm[20]. The encapsulation efficiency of the PCL particles containing 0.1, 0.25, 0.5, and 1% wt v^{-1} of CaO_2 was determined as 64.6 ± 2.3 %, 63.2 ± 3.4 %, 68.0 ± 1.2 %, and 72.3 ± 4.1 % respectively, (Figure 2d). An increase in the CaO_2 concentration results in a higher encapsulation efficiency and an increase in the CaO_2 loading content (Figure 2e). This trend has been previously observed in the case of poly(lactic acid) (PLLA) particles, where an increase in the CaO_2 concentration from 0.2 to 0.5 wt%, with a constant PLLA concentration, resulted in an increased encapsulation efficiency[11].

The distribution of the loaded CaO_2 within the PCL particles was analyzed using alizarin red staining. Figures 2f and j indicated that CaO_2 was encapsulated within the PCL particles. However, the CaO_2 was not uniformly distributed throughout the particles. This non-uniform distribution of CaO_2 is also reported in particles synthesized through different methods such as electrospray and oil/water phase methods[20, 38]. After evaluating the encapsulation efficiency and CaO_2 loading, the P1 particles with the highest CaO_2 loading content of 6.9 ± 1.7 % were selected for further O_2 release and kinetic studies.

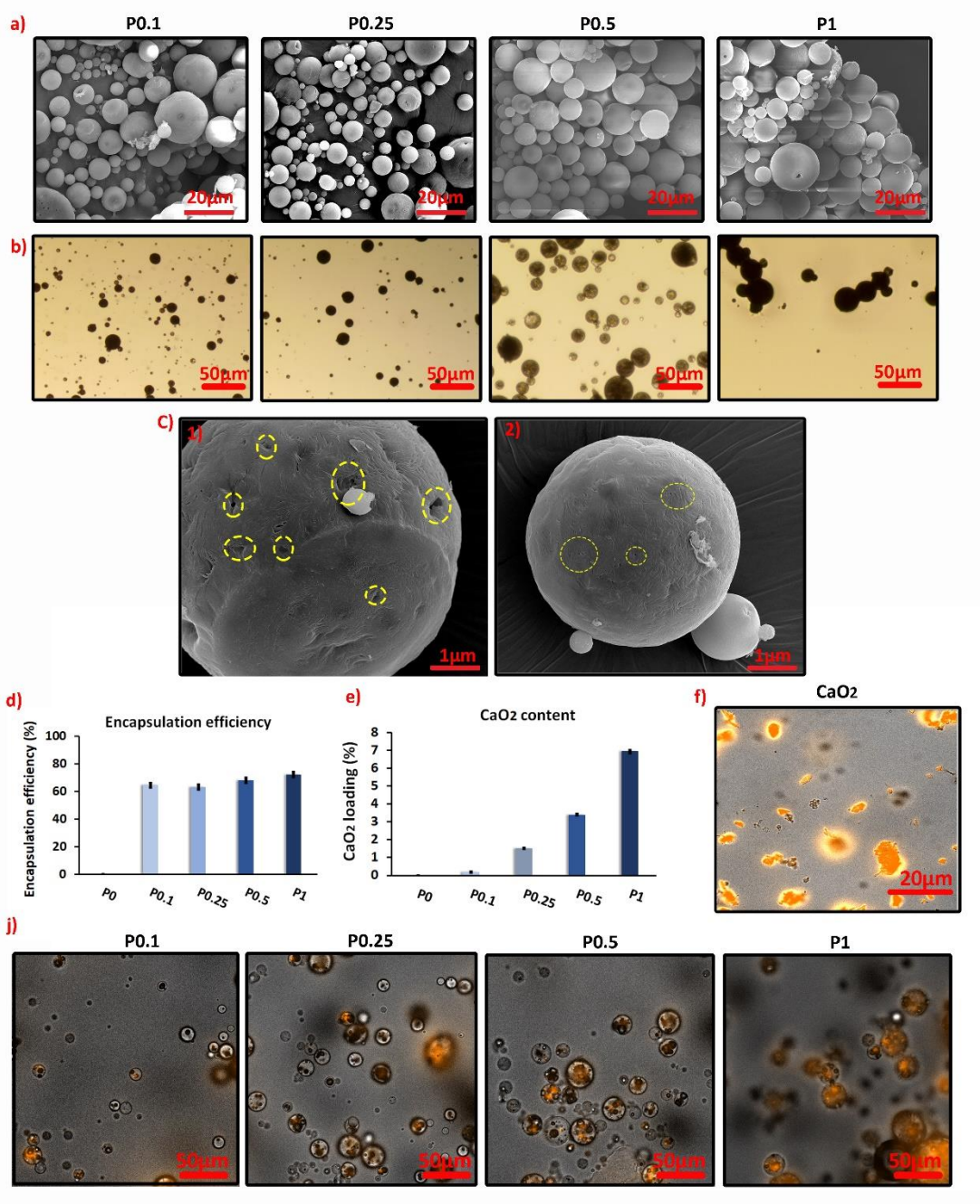

Figure 2. (a) SEM micrograph images of P0.1, P0.25, P0.5, and P1 wt v^{-1} particles, (b) Microscopic images of P0.1, P0.25, P0.5, and P1 wt v^{-1} particles, (c 1 and 2) SEM micrograph images of P1 wt v^{-1} particles, pores were circled in yellow, (d) encapsulation efficiency (wt wt^{-1} %), (e) CaO_2 loading content (wt wt^{-1} %), and (f and j) fluorescent images of CaO_2 and P0.1, P0.25, P0.5, and P1 wt v^{-1} particles stained with alizarin red to investigate the distribution of incorporated CaO_2 into the particles.

3.2 Characterization of the PFC-chitosan

The conjugation of PFC groups on the chitosan chains occurs via Schiff base formation or nucleophilic substitution between the free primary amino groups of the chitosan and chloride of the PFCs[22]. The acidic media of the reaction leads to a preferentially favored reaction for primary amine instead of hydroxyl groups in the chitosan[22]. The presence of PFCs on chitosan was indicated by the appearance of four peaks between -125 to -79 ppm in the ^{19}F NMR spectra of PFC-chitosan (Figure 3a). The substitution degree of PFC on the chitosan was calculated to be 39.8%. It has been reported that the cytotoxicity of the modified chitosan and methacrylated chitosan with PFCs increases with a substitution degree greater than 37-42%[22, 23, 30]. The results of the ^{1}H NMR confirmed the attachment of PFCs to the chitosan chain, as indicated by a chemical shift in the peak related to the nearest carbon-hydrogen to the primary amines of chitosan (C-H) (represented in pink in the chitosan structure, Figure 3b). The peak shifted from 3.15 ppm before conjugation to 3.37 ppm after conjugation (Figure 3b). The sharp peaks at 1.98 and 3.85 ppm in the ^{1}H NMR of PFC-chitosan are attributed to deuterated THF.

FTIR spectra of PFC-chitosan exhibited two peaks at 1146 and 1202 cm^{-1}, which were attributed to the fluoro compound (Figure 3c)[39]. Additionally, two peaks related to the symmetric and asymmetric stretching of primary amines of the chitosan, which were dominant over hydroxyl group peaks, were observed at 3277 and 3351 cm^{-1}[40, 41].

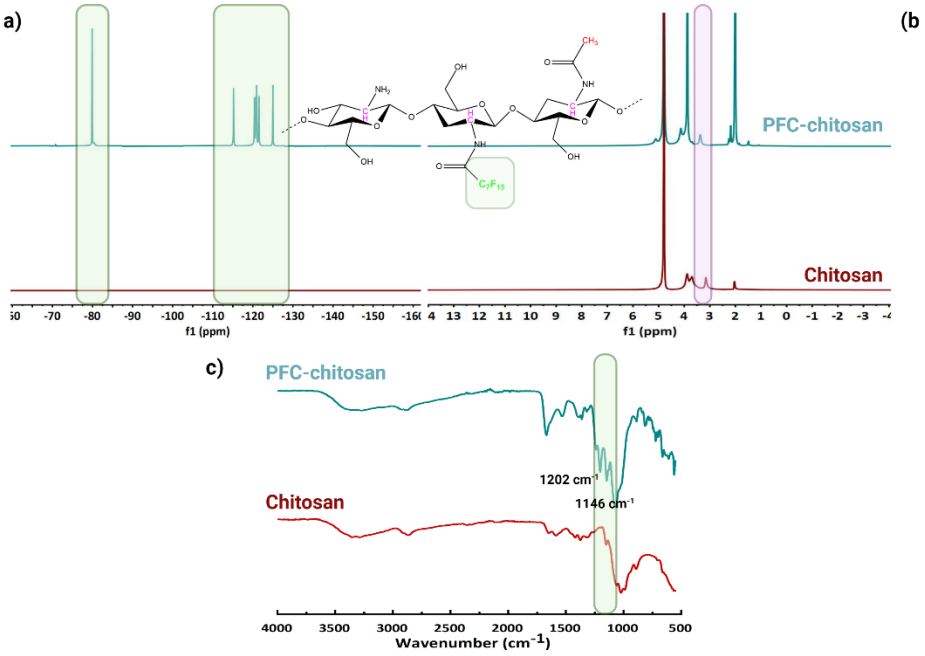

Figure 3. (a) ^{19}F NMR, (b) ^{1}H NMR and (c) FTIR of the chitosan and the PFC-chitosan film.

3.3 Morphology, topography, hydrophilicity, and degradation of the films containing particles

The AFM results of the chitosan, PFC-chitosan, and PFC-chitosan containing P1 (1:1 wt wt^{-1}) films are presented in Figure 4a. While the chitosan film and PFC-chitosan displayed uniform structures[42], the roughness of the PFC-chitosan surface was heightened by the incorporation of the particles. The height difference between the peaks and valleys of the PFC-chitosan-containing particles was ≥ 300 nm, whereas the height difference for the chitosan and PFC-chitosan film was ≤ 30 nm. The presence of the particles on the surface of the films was also observed by the SEM images (Figure 4b).

The surface and bulk hydrophilicity of chitosan, PFC-chitosan, and P1/PFC-chitosan films were studied to understand the impact of PFC-chitosan's hydrophobicity on the O_2 release rate. The water contact angle (WCA) was measured as an indicator of hydrophilicity. The substitution of the free amines groups in the chitosan with hydrophobic fluorine groups was found to increase the WCA from 73°±3 to 103°±2 (Figure 4c). the chitosan modification with PFC also led to a reduction in the film swelling ratio, causing a decrease in water uptake by 22.2% in comparison to the pure chitosan film.

The incorporation of CaO_2-loaded PCL particles had no noticeable effect on the surface hydrophilicity of the film and the WCA remained 95°±2. However, the swelling of PFC-chitosan-containing particles was higher than that of the PFC-chitosan film at all tested time points. This could be attributed to the creation of porosities caused by incorporating the particles into the film, which can increase the swelling ratio of the PFC-chitosan/particle film (Figure 4d).

Conjugating of PFCs on chitosan decreased the degradation rate of chitosan, and the ultimate mass loss percentage of chitosan and PFC-chitosan was 40.1 and 29.9%, respectively (Figure 4e). Therefore, the PFC groups with a hydrophobic nature reduced the hydrophilicity and increased the stability of the chitosan film. The bond between carbon-fluorine with an energy bond of 450 kJ/mol is known as the strongest existing covalent bond. Furthermore, each fluorine atom is surrounded by 3 pairs of nonbonding electrons, which make them stable[43]. Therefore, PFCs are resistant to degradation by bases, acids, reductants, oxidants, photolytic, microbes, and metabolic processes with a half-life of approximately 2 to 8 years in the human body [44]. PFC

compounds are generally safe for biomedical applications where the material is not intended for long-term exposure to a body which results in accumulation in tissue such as the liver or blood. The observed degradation associated with PFC-chitosan films can be attributed to the degradation of chitosan rather than PFC.

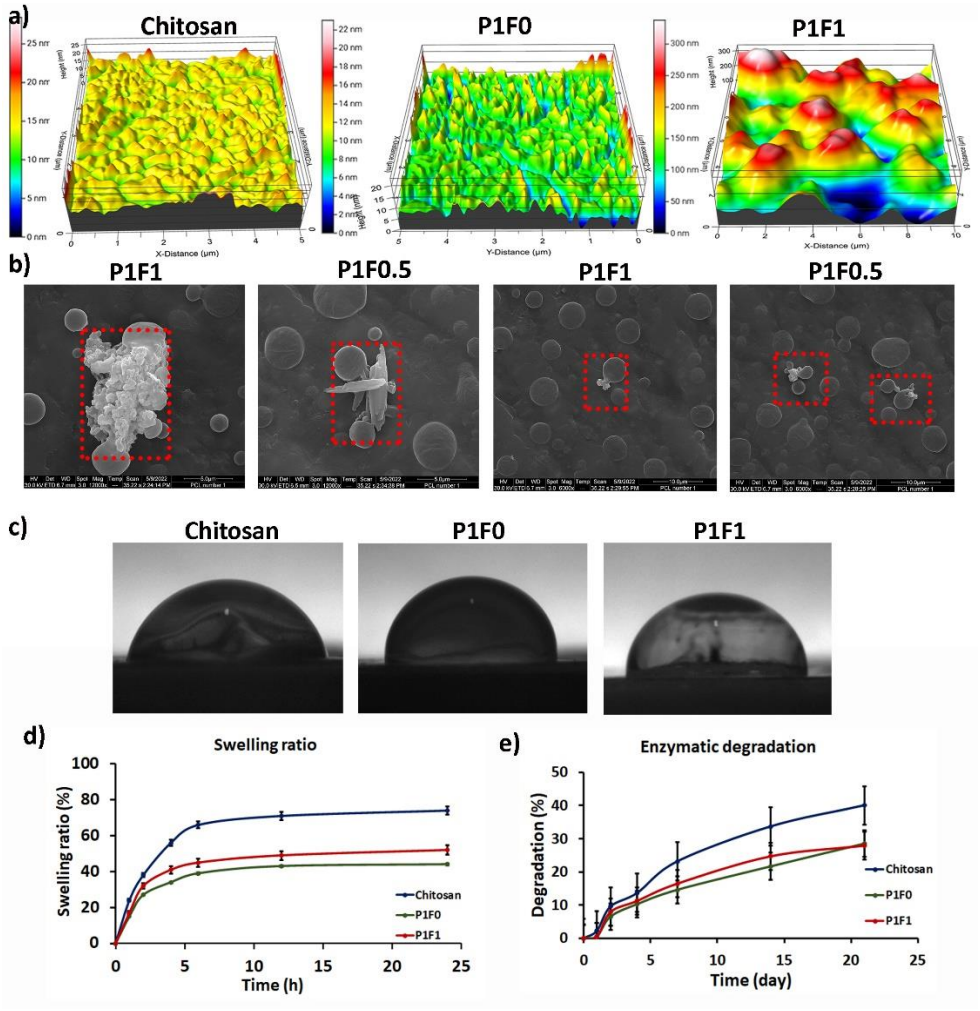

Figure 4. (a) SEM of the surface of P1F1 and P1F0.5 films with two magnifications 6000X and 12000X, (b) AFM of chitosan, P1F0, and P1F1, (c) WCA, (d) swelling ratio (%), and (e) degradation of chitosan, P1F0, and P1F1 films.

3.4 Release and kinetics of O_2 and H_2O_2 from the particles

According to Equations 6 and 7, the decomposition of CaO_2 can lead to the production of O_2 and H_2O_2. To evaluate the impact of encapsulating CaO_2 within a hydrophobic shell (in this

case PCL), the release and kinetics of O_2 and H_2O_2 generated from the P1 particles were compared with those generated from uncoated CaO_2.

$$CaO_2 + H_2O \rightarrow Ca(OH)_2 \downarrow + \frac{1}{2}O_2 \uparrow \quad (6)$$

$$CaO_2 + 2H_2O \rightarrow Ca(OH)_2 \downarrow + H_2O_2 \quad (7)$$

3.4.1 Effect of normoxia

The concentration of O_2 in the solution and gas phases and H_2O_2 in the solution phase increased upon the addition of CaO_2 and P1 particles to the release media (Figure 5a-c, and Table 3). This simultaneous generation of O_2 and H_2O_2 from CaO_2 was previously documented by Wang et al.[19] Furthermore, Wu et al. and Hsieh et al. have demonstrated that the incorporation of CaO_2 into hollow mesoporous silica nanoparticles with polyacrylic acid and poly lactic-co-glycolic acid microparticles, respectively, results in the generation of O_2 and H_2O_2 upon introduction to PBS[45, 46].

The cumulative H_2O_2 concentration generated by 15mg of CaO_2 reached a maximum of 632.80 µM after 80 minutes, which marks the "termination time" of CaO_2 and signifies the point when its decomposition ceased (Figure 5c and Table 3)[19]. The H_2O_2 concentration remained constant until the 48^{th} hour (Figure 5c). Likewise, it has been demonstrated that the reaction of CaO_2 with water results in the immediate generation of H_2O_2, leading to a rapid increase in the cumulative concentration of H_2O_2, which subsequently stabilizes at a constant level[45-48]. For example, the reaction of 100 mg of CaO_2 with water at room temperature generated 75 µM of H_2O_2 immediately[47] and the cumulative concentration of H_2O_2 remained stable at this level for 7 hours[47].

Two primary factors have been proposed to account for the rapid termination of CaO_2 decomposition. The first is the elevation of the pH level in the H_2O_2 release medium, which results from the generation of calcium hydroxide as a secondary product of the CaO_2 (Equations 6 and 7) decomposition and therefore increases the pH of the media[49]. In our work, during the release study, the pH of the release media (DI water) increased from 7.4 to 9.8 by CaO_2 decomposition.

Secondly, the rate of H_2O_2 release can be regulated by its diffusion through the solid layers of calcium hydroxide[49, 50]. Additionally, although CaO_2 decomposition produces O_2, the

pressure in the solution phase remained constant at 1 bar, which was measured by the O_2 analyzer. Therefore, the rapid termination time of CaO_2 release cannot be attributed to changes in the pressure within the release medium, as predicted by Le Chatelier's principle.

The hydrophobic PCL shell extended the termination time of CaO_2 by preventing CaO_2 from decomposition by DI water[46, 47]. The H_2O_2 concentration generated by P1 particles continued to increase with reaction time and reached 150.32 µM after 48 hours in the release media (Figure 5c and Table 3). Within 48 hours, the pH of the release media in the presence of P1 and CaO_2 increased to 8.6 and 9.8 respectively which showed the efficacy of PCL in P1 particles in impeding water access to CaO_2.

A report has indicated that covering the CaO_2 with lauric acid could shield CaO_2 from reacting with water and decrease the cumulative H_2O_2 release from 75 µM to 30 µM [47]. Furthermore, Hsieh et al. have noted that there is a direct correlation between the concentration of the CaO_2 encapsulation material and the concentration of H_2O_2[46]. Specifically, the concentration of H_2O_2 decreased from ~170 µM to 50 µM as the concentration of poly(lactic-co-glycolic acid) was increased from 5 to 20%. No H_2O_2 was detected in the release media containing P0 particles, suggesting that the detected H_2O_2 was a result of the decomposition of CaO_2.

Moreover, the hydrophobic PCL shell extend the O_2 release time and decreased the O_2 yield (Table 3). The maximum O_2 concentration from CaO_2 was recorded at the same time as the termination time of CaO_2 (Figure 5a), as determined from the H_2O_2 release pattern (Figure 5c). The slower and lower O_2 release from P1 particles, compared to CaO_2, might have allowed the generated O_2 molecules to dissolve in the solution phase and transfer to the gas phase more gradually, resulting in a shorter and slower drop in O_2 concentration for P1 particles compared to CaO_2 (Figure 5a). A similar pattern has been reported for O_2 release by covered CaO_2 by lauric acid [47] and poly(lactic-co-glycolic acid) [46] compared to CaO_2.

3.4.2 Effect of hypoxia

Under hypoxia conditions, the O_2 generated via CaO_2 decomposition is rapidly consumed by surrounding media and therefore the decomposition rate of CaO_2 was faster than under normal O_2 levels due to the increased driving force (ΔO_2) in hypoxia (Figures 5d-f). Similarly, Colombani et al. showed that the release rate of O_2 from CaO_2 incorporated into a cryogel based on methacrylated hyaluronic acid was 2 µM h^{-1} higher in hypoxia than in normoxia[51].

The termination time of CaO_2 was found to be 50 minutes in hypoxia, a decrease of 30 minutes from the termination time in normoxia (Figures 5d and e and Table 3).

Due to the faster release of O_2 from CaO_2 and P1 particles in hypoxia, the decrease in O_2 concentrations after the maximum release was faster and higher than in normoxia (Figure 5a and 5e, and Table 3). Liu et al. have previously reported that the concentration of O_2 from CaO_2 was reduced more than the covered CaO_2 by lauric acid after reaching the maximum O_2 concentration [47].

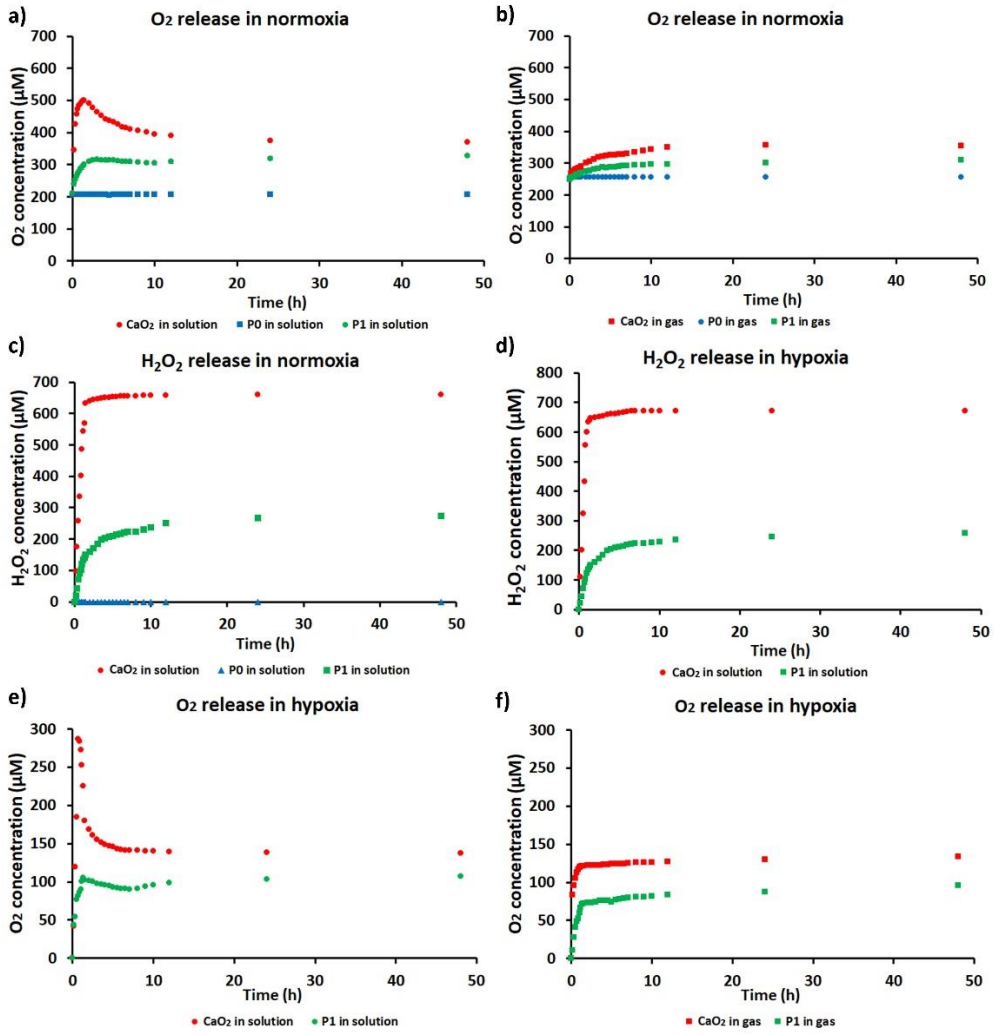

Figure 5. (a) O_2 release from CaO_2, P0, and P1 particles in normoxia in the solution phase (the initial concentration of O_2 in the solution phase was approximately 205 μM), (b) O_2 release from CaO_2, P0, and P1 particles in normoxia in the gas phase (the initial concentration of O_2 in the gas phase was approximately 250 μM), (c) H_2O_2 release from CaO_2, P0, and P1 particles in

480 normoxia in the solution phase, (d) H_2O_2 release from CaO_2 and P1 particles in hypoxia in the
481 solution phase, (e) O_2 release from CaO_2 and P1 particles in hypoxia in the solution phase, and (f)
482 O_2 release from CaO_2 and P1 particles in hypoxia in the gas phase.

483 *3.4.3 Effect of the different volumes of the release media*

484 We monitored the concentration of O_2 in both the solution and gas phases for 25 mL and
485 50 mL release media volumes and only in the liquid phase for the 100 mL volume due to the lack
486 of space for the gas phase (Figures 6a and b).

487 Results showed that the cumulative concentration of H_2O_2 generated from CaO_2 and P1
488 particles was similar and unchanged by the volume of the release media (Figure 6a and Table 3).
489 The termination time of CaO_2 was determined to be 50 minutes, consistent with the termination
490 time under the hypoxia condition.

491 Reducing the release media volume decreased the O_2 concentration in the solution but
492 increased the O_2 concentration in the gas phase. However, the total amount of O_2 generated from
493 a constant amount of CaO_2 remained unaffected (Figures 6b and d, and Table 3). A decrease in O_2
494 concentration was observed at 25 mL and 50 mL due to the transfer of O_2 from the solution phase
495 to the gas phase, but not at 100 mL due to the full volume of the reactor with the solution phase
496 (Figure 6c and d, and Table 3).

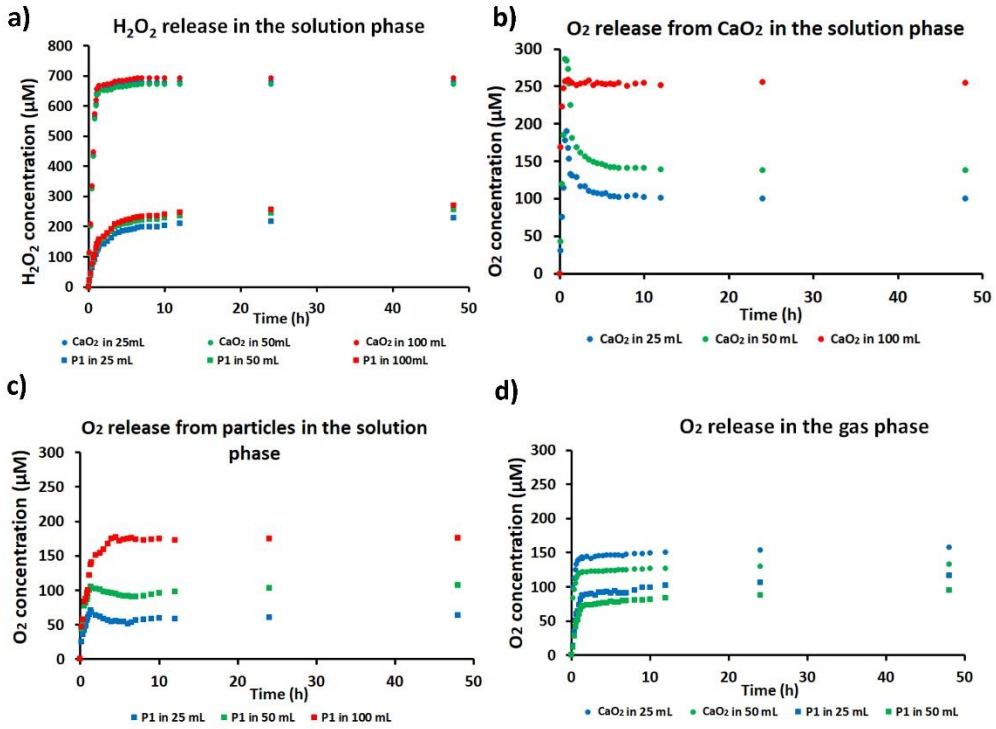

Figure 6. (a) H_2O_2 release from CaO_2 and P1 particles in 25, 50, and 100 mL of the solution phase, (b) O_2 release from CaO_2 in 25, 50, and 100 mL of the solution phase, (c) O_2 release from P1 particles in 25, 50, and 100 mL of the solution phase, and (d) O_2 release from CaO_2 and P1 in the gas phase when the volume of the solution phase is 25 and 50 mL.

3.4.4 Effect of the amount of CaO_2

As the initial amount of CaO_2 increased, the concentration of O_2 and H_2O_2 increased (Figures 7a-d). The cumulative concentration of H_2O_2 from CaO_2 and P1 increased by increasing the amount of CaO_2 (Table 3). As previously reported[19], an increase in H_2O_2 concentration was observed over a longer period as the amount of CaO_2 increased.

The termination time of CaO_2 based on O_2 concentration from CaO_2 shifted to shorter times. The termination time for 5 mg of CaO_2 was 66 min, while that for 25 mg was 45 min. The H_2O_2 and O_2 release from CaO_2 confirms the previous report indicating that the release patterns of H_2O_2 and O_2 from CaO_2 follow pseudo-zero-order and pseudo-first-order kinetics, respectively[19]. This difference in the rate of O_2 release may be due to the reactant being solid CaO_2 instead of CaO_2 dissolved in water[19].

The concentration of O_2 and H_2O_2 gradually increased over time as the release media penetrated the inner part of the P1 particles through nanosized porosities (as depicted in Figure 2c and from the gas adsorption results), and the trapped CaO_2 was decomposed. We acknowledge that the nanosized porosities play a significant role in the water permeation rate through the particles and decomposition rate. On the other hand, it is challenging to achieve control over the size of porosities during the synthesis process using water/oil precipitation. Therefore, the limitation of this work is to study the impact of the size of porosities on the CaO_2 decomposition rate.

Table 2 summarizes some of the methods used to mitigate the decomposition of CaO_2 along with their corresponding initial release outcomes. The methods that have a short initial O_2 release are used for cancer therapy, while the methods that have an extended O_2 release time are utilized for wound healing and angiogenesis.

Table 2. Summary of CaO_2 protecting methods and materials along with their initial release.

Protecting materials	**Developed materials**	**Method**	**Dissolved O_2 (mmol/L)**	**Time of initial release**	**Ref**
PCL	Particles	Electrospray	~ 31	1 day (first measured time point)	[52]
PLLA	Particles	$W_1/O/W_2$	~ 0.23	1 day (first measured time point)	[11]
Poly lactic-co-glycolic acid	Particles	Oil/ water	~ 0.312-0.54	12 hours	[46]
Polyethylene glycol	Particles	-	~ 0.37- 0.43	90 minutes (first measured time point)	[49]
Lauric acid	Particles	-	~ 0.312-0.15	2 minutes	[47]
Polyacrylic acid	Particles	-	Less than 1	3 hours	[45]
PCL	Particles	Oil/water	~ 0.15 mmol/L	4.5 hours	This work

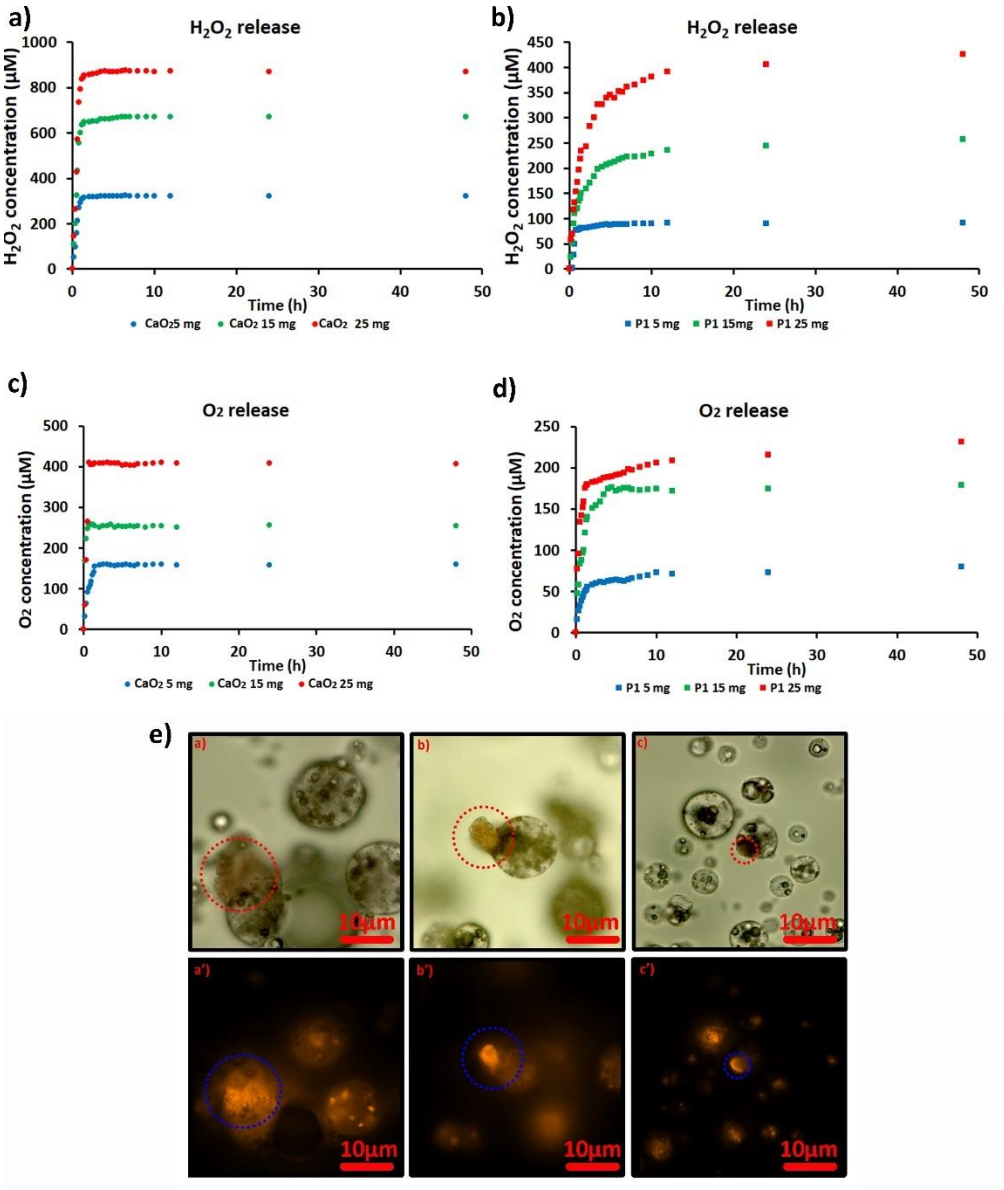

Figure 7. (a) H_2O_2 release from 5, 15, and 25 mg of CaO_2, (b) H_2O_2 release from a certain amount of P1 particles containing 5, 15, 25 mg CaO_2, (c) O_2 release from 5, 15, and 25 mg of CaO_2, (d) O_2 release from a certain amount of P1 particles containing 5, 15, 25 mg CaO_2, and (e) the microscopic (a-c) and fluorescent images (a'-c') of the loaded CaO_2 in the outer layer of the PCL particles.

3.4.5 Effect of catalase

H_2O_2 as low as 30 µM has also been reported to exhibit cytotoxicity[53, 54]. An excessive generating of H_2O_2 leads to oxidative stress and cell damage [55]. The release of O_2 from P1 particles was investigated in the presence of catalase. The use of catalase may decrease the

potential toxicity of H_2O_2 for cells and wound healing, and increase the efficiency of the particles in O_2 generation by decomposing H_2O_2 to O_2.

$$2\ H_2O_2 \rightarrow 2\ H_2O + O_2 \quad (8)$$

The decomposition of H_2O_2 to O_2 is mediated by a two-step mechanism that is dependent on the specific type of catalase under examination. The mechanism involves the oxidation of the heme cofactor through the use of a single molecule of H_2O_2, resulting in the formation of an oxyferryl species (Equation 9). This process leads to breaking O-O bond of the H_2O_2, creation of a porphyrin cation radical intermediate, and forming water. In the subsequent stage, the intermediate (compound I) is reduced by a second molecule of H_2O_2, resulting in the regeneration of the resting state enzyme and the release of water and O_2 (Equation 10) [56].

$$\text{Enz } (Por^{+\bullet}\text{–}Fe^{III}) + H_2O_2 \rightarrow \text{Cpd I } (Por^{+\bullet}\text{–}\ Fe^{IV}\text{=O}) + H_2O \quad (9)$$

$$\text{Cpd I } (Por^{+\bullet}\text{–}Fe^{IV}\text{=O}) + H_2O_2 \rightarrow \text{Enz } (Por\text{–}Fe^{III}) + H_2O + O_2 \quad (10)$$

The effect of catalase on the O_2 and H_2O_2 release of CaO_2 and P1 particles was studied under hypoxia in 100 mL of the release media at pH 7.4, and room temperature. The results showed that the presence of catalase accelerated and increased the O_2 release from both CaO_2 and P1 particles (Figures 8a, b, and Table 3).

According to the concentration of H_2O_2 and O_2 from CaO_2 and P1 with and without catalase, the concentration of O_2 produced from CaO_2 and P1 particles with catalase was close to the sum of O_2 concentration generated from the CaO_2 and P1 without catalase and the theoretical amount of O_2 that can be produced by the released H_2O_2 from them (Table 3). Therefore, catalase could enhance the efficiency of the PCL particles in producing O_2 by decomposing the generated H_2O_2. No H_2O_2 was detected from the release media containing catalase.

The concentration of O_2 from P1 particles increased progressively until 96 hours and then was constant for 2 days, which marked the termination time of loaded CaO_2 into PCL particles (Figure 8c).

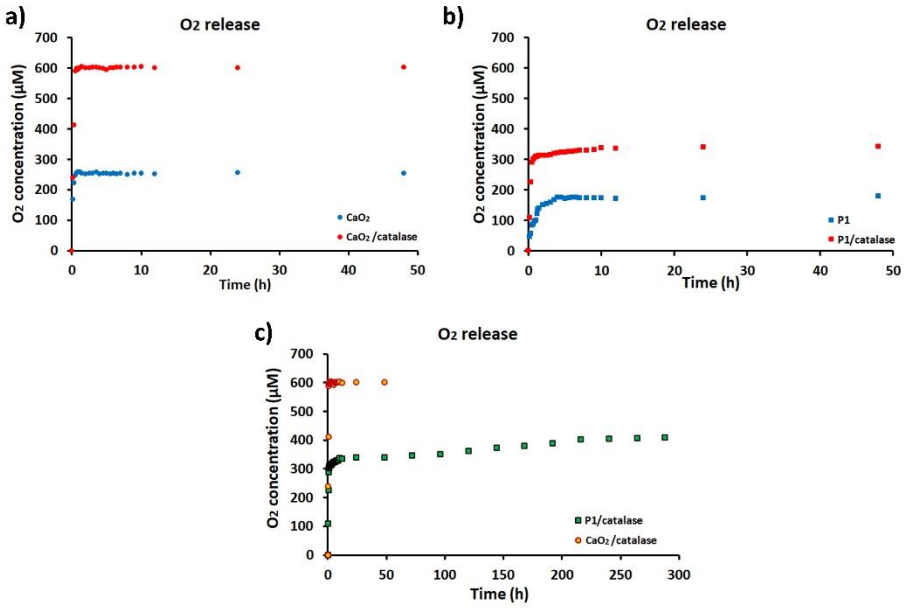

Figure 8. (a) O_2 release from 15 mg of CaO_2 with and without catalase in 100 mL of DI water, (b) O_2 release from a certain amount of P1 particles containing 15 mg of CaO_2 with and without catalase in 100 mL of DI water, (c) O_2 release from 15 mg of CaO_2 and a certain amount of P1 particles containing 15 mg of CaO_2 with catalase until 288 hours.

Table 3. Summary of the concentration of O_2 and H_2O_2 released from CaO_2 and P1 under different conditions.

Sample	**Amount of CaO_2 (mg)**	**Release condition**					**Max. O_2 in the solution phase (μM)**	**Equilibrium O_2 in the solution phase (μM)**	**Max. O_2 in the gas phase (μM)**	**Equilibrium O_2 in the gas phase (μM)**	**Max. H_2O_2 (μM)**
		pH	T (℃)	Initial O_2 concentration (%)	The volume of released media						
					Solution (mL)	Gas (mL)					
CaO_2	15	7.4	RT*	Normoxia	50	50	498.76	371.00	354.71	354.71	632.80
P1	15	7.4	RT	Normoxia	50	50	314.99	327.51	309.03	309.03	279.90
CaO_2	15	7.4	RT	Hypoxia	50	50	283.74	137.80	133.34	133.34	672.10
P1	15	7.4	RT	Hypoxia	50	50	102.68	107.31	95.33	95.33	256.90
CaO_2	15	7.4	RT	Hypoxia	25	75	189.61	99.85	157.32	157.32	680.29
CaO_2	15	7.4	RT	Hypoxia	100	0	254.63	254.63	-	-	692.93
P1	15	7.4	RT	Hypoxia	25	75	71.25	63.78	116.30	116.30	228.51
P1	15	7.4	RT	Hypoxia	100	0	175.32	175.32	-	-	269.61

CaO_2	5	7.4	RT	Hypoxia	100	0	159.65	159.65	-	-	322.40
CaO_2	25	7.4	RT	Hypoxia	100	0	406.05	406.05	-	-	871.37
P1	5	7.4	RT	Hypoxia	100	0	79.63	79.63	-	-	91.26
P1	25	7.4	RT	Hypoxia	100	0	231.04	231.04	-	-	425.59
CaO_2/catalase	15	7.4	RT	Hypoxia	100	0	602.15	602.15	-	-	-
P1/catalase	15	7.4	RT	Hypoxia	100	0	408.83	408.83	-	-	-
P1F0.5	15	7.4	RT	Hypoxia	100	0	158.67	158.67	-	-	200.32
P1F1	15	7.4	RT	Hypoxia	100	0	162.92	162.92	-	-	222.98

*RT means room temperature.

3.4.6 Kinetic of O_2 and H_2O_2 release from the particles

The kinetics of O_2 and H_2O_2 from CaO_2 were investigated from t_0 to the termination time of CaO_2. The kinetics related to P1 was calculated in the first 5 hours, where the particles showed rapid release.

The kinetic of generated O_2 and H_2O_2 from CaO_2 decomposition is a heterogeneous reaction. According to the release of H_2O_2 with different amounts of CaO_2 and P1 particles (Figure 7a and b), the apparent release rate of H_2O_2 ($r_{H_2O_2}$) may follow a pseudo-zero-order kinetic pattern, where the rate of the reaction is independent of the concentration of one or more reactants. In this case, the rate of H_2O_2 release may not be affected by the concentration of CaO_2, but rather by the surface area of the solid and is described by the following Equation:[19]

$$r_{H_2O_2} = \left(\frac{d(C_{H_2O_2})}{dt}\right) = k_{H_2O_2} \times \left(C_{CaO_2}\right)^0 \quad (11)$$

Where t is the release time, and $C_{H_2O_2}$ is the concentration of H_2O_2 at different times. As shown in Figure 9a, the H_2O_2 concentration from P1 particles with different amounts of CaO_2 grew with the same trend. All the release curves fitted the pseudo-zero-order kinetic ($R^2 \geq 95$). The constant release rates of H_2O_2 ($k_{H_2O_2}$) showed a change at about 1 h for all the particles, which was equal to the termination time of CaO_2 in hypoxia.

Therefore, the kinetic of the released H_2O_2 from the particles could be divided into two parts with different rates. Part 1: t_0=zero to t_1= the termination time of CaO_2; part 2: t_1 to t_2 = end of the rapid release (Figure 9a-h and Table 4). The $k_{H_2O_2}$ of P1 particles containing 5, 15, and 25

mg of CaO_2 was approximately the same in part 1 (Table 4), which shows the independency of the kinetic of H_2O_2 to the initial amount of CaO_2[19].

In contrast, the generated O_2 from the decomposition of loaded CaO_2 in the PCL particles is affected by the CaO_2 amount and follows a pseudo-first-order reaction (Figure 9b) where the rate of the O_2 generation is proportional to the concentration of the limiting reactant (the loaded CaO_2). According to Equations 6 and 7, CaO_2 is consumed to generate O_2 and H_2O_2 so that the CaO_2 amount at each reaction time define by subtracting the consumed CaO_2 in both reactions (Equations 6 and 7) from the initial CaO_2 amount[19]. Therefore, the CaO_2 amount at each reaction moment will be $C_0 - C_{H_2O_2} - 2C_{O_2}$. Where "$C_0$" is the initial amount of CaO_2 (M). Hence the O_2 rate (r_{O_2}) can be determined by Equation (12)[19].

$$r_{O_2} = \frac{d(C_{O_2})}{dt} = \frac{1}{2} k_{O_2} \left(\frac{C_0 - C_{H_2O_2} - 2C_{O_2}}{dt}\right) \quad (12)$$

Where k_{O_2} is constant of the apparent O_2 release rate. Equation 12 can be transformed into Equation 13[19], in which its slope determines the k_{O_2}.

$$-\mathrm{Ln}\left(\frac{C_0 - C_{H_2O_2} - 2C_{O_2}}{C_{O_2}}\right) = k_{O_2} \times t \quad (13)$$

The proposed model suggests that the amount of CaO_2 has a significant influence on the rate of O_2 release. It is evident that the natural logarithm of the ratio between the remaining CaO_2 and the concentration of O_2 follows a linear relationship with time, with the slope representing the rate constant (k_{O_2}). Therefore, the value of k_{O_2} at the time "t" is influenced by the initial amount of CaO_2, as well as the concentrations of generated H_2O_2 and O_2 at that specific time. Our results demonstrate that increasing the initial amount of CaO_2 leads to an increase in k_{O_2}, as depicted in Figure 9b. The kinetic behavior of O_2 release differs from that of H_2O_2 release, which follows a pseudo-zero order reaction pattern. This disparity is believed to be due to the nature of the reactant involved in the O_2 release process, particulate CaO_2, as opposed to dissolved CaO_2 in water. As a consequence, the concentration of CaO_2 in the slurry can have a direct impact on the reaction, as reported in[19].

Figures 9c and d depict the kinetics of O_2 and H_2O_2 release under hypoxia and normoxia at room temperature, pH of 7.4, and a solution volume of 100 mL. The results demonstrated that

hypoxia accelerated the decomposition rate of CaO_2, increasing the rate constants ($k_{H_2O_2}$ and k_{O_2}) (Table 4). The higher value of $k_{H_2O_2}$ compared to k_{O_2} under the same conditions suggests that the dominant reaction in the CaO_2 decomposition is the generation of H_2O_2 (Table 4), as stated by wang et al[19].

Under hypoxic conditions, the rate of O_2 and H_2O_2 generation from P1 particles increased in both parts. In part 1, the rapid release of O_2 and H_2O_2 was attributed to the decomposition of partially covered CaO_2, as demonstrated by the simultaneous changes in the rate constants ($k_{H_2O_2}$ and k_{O_2}) at the termination of CaO_2. In contrast, in part 2, the growth of O_2 and H_2O_2 concentrations was slower, as water penetrated the PCL particles via nanoscale pores on their surface and reacted with the encapsulated CaO_2.

Table 4. $k_{H_2O_2}$ and k_{O_2} related to the CaO_2 and P1 particles in hypoxia and normoxia.

Samples	k_{O_2} ($\mu M^{-1} h^{-1}$)		$k_{H_2O_2}$ ($\mu M^{-1} h^{-1}$)	
	Part 1	Part 2	Part 1	Part 2
CaO_2 in normoxia	0.992	-	458.760	-
CaO_2 in hypoxia	1.194	-	675.600	-
P1 in normoxia	0.164	0.020	107.550	24.430
P1 in hypoxia	0.249	0.025	149.650	25.570

Since wounds can have different pH [17] and temperature [18], the final yield and kinetic of H_2O_2 and O_2 from P1 particles were explored in various pHs (6, 7.4, and 9) and temperatures (room temperature and 37 °C) under hypoxia (Figure 9e-h).

The changes in k_{O_2} and $k_{H_2O_2}$ were closely linked to the termination time of CaO_2 decomposition, as shown in Table 5. By increasing the pH from 6 to 9 at a given temperature, the k_{O_2} and $k_{H_2O_2}$ decreased (Figure 9e-h and Table 5). Moreover, increasing the temperature at a given pH accelerated the O_2 and H_2O_2 release rate (Table 5).

The yield of O_2 increased and the yield of H_2O_2 decreased as the pH was raised at a constant temperature. In addition, increasing temperature at a fixed pH resulted in an increase in O_2 yield and a decrease in H_2O_2 yield. The improvement in O_2 yield at higher temperatures and pH could be attributed to the decomposition of H_2O_2[19]. It is suggested that the thermal decomposition process could accelerate the decomposition of H_2O_2 at elevated temperatures[57]. It is

hypothesized that the release of H_2O_2 from CaO_2 occurs through a two-step mechanism. First, CaO_2 decomposes when in contact with water, forming peroxide (O_2^{2-}) and calcium (Ca^{2+}) ions. Second, the generated O_2^{2-} reacts with hydrogen ions (H^+) to produce H_2O_2. In an acidic environment, characterized by an abundance of H^+ ions, the decomposition of CaO_2 is enhanced, increasing in k_{O_2}, as evidenced in Table 5.

Moreover, previous research by Wang et al.[19] has proven that the plot of $\ln k_{O_2}$ versus 1/T for CaO_2 decomposition follows a linear relationship. Therefore an increase per degree of temperature can lead to an increase in the k_{O_2}. When temperature increases, the exponential term in the Arrhenius Equation becomes more significant, leading to an increase in the rate constant. This is due to the greater thermal energy available to the reacting molecules, resulting in higher collision frequencies and more successful collisions with sufficient energy to overcome the activation energy barrier.

During the inflammatory phase of an acute wound, the wound temperature increases due to infection and inflammation[58]. Hence, CaO_2-loaded PCL particles can supply more O_2 with a higher k_{O_2} in an infected wound than a normal wound. Furthermore, bacteria present in the wound environment produce ammonia, resulting in an alkaline wound, which can increase the O_2 yield from the CaO_2-loaded PCL particles. However, the rate of increase is slower compared to that of a wound with an acidic pH.

The release of H_2O_2 from CaO_2-loaded particles was the dominant reaction. This aligns with previous findings that the CaO_2 decomposition reaction is influenced by pH and temperature, and also H_2O_2 being the major product[19]. Thus, the incorporation of CaO_2 into a hydrophobic shell did not alter the CaO_2 decomposition reaction. However, the hydrophobic shell extended the duration of the decomposition reaction.

Table 5. k_{O_2} and $k_{H_2O_2}$ of the generated O_2 and H_2O_2 from P1 particles under various temperatures and pHs.

pH	k_{O_2} (μM^{-1} h^{-1})		$k_{H_2O_2}$ (μM^{-1} h^{-1})	
	RT*	37°C	RT*	37°C
P1, pH of 6, part 1	0.375	0.567	209.400	323.790
P1, pH of 7.4, part 1	0.249	0.270	149.650	268.270

P1, pH of 9, part 1	0.174	0.199	99.600	123.210
P1, pH of 6, part 2	0.025	0.033	24.306	24.727
P1, pH of 7.4, part 2	0.025	0.032	25.570	25.791
P1, pH of 9, part 2	0.015	0.021	20.641	16.945

666 *RT means room temperature

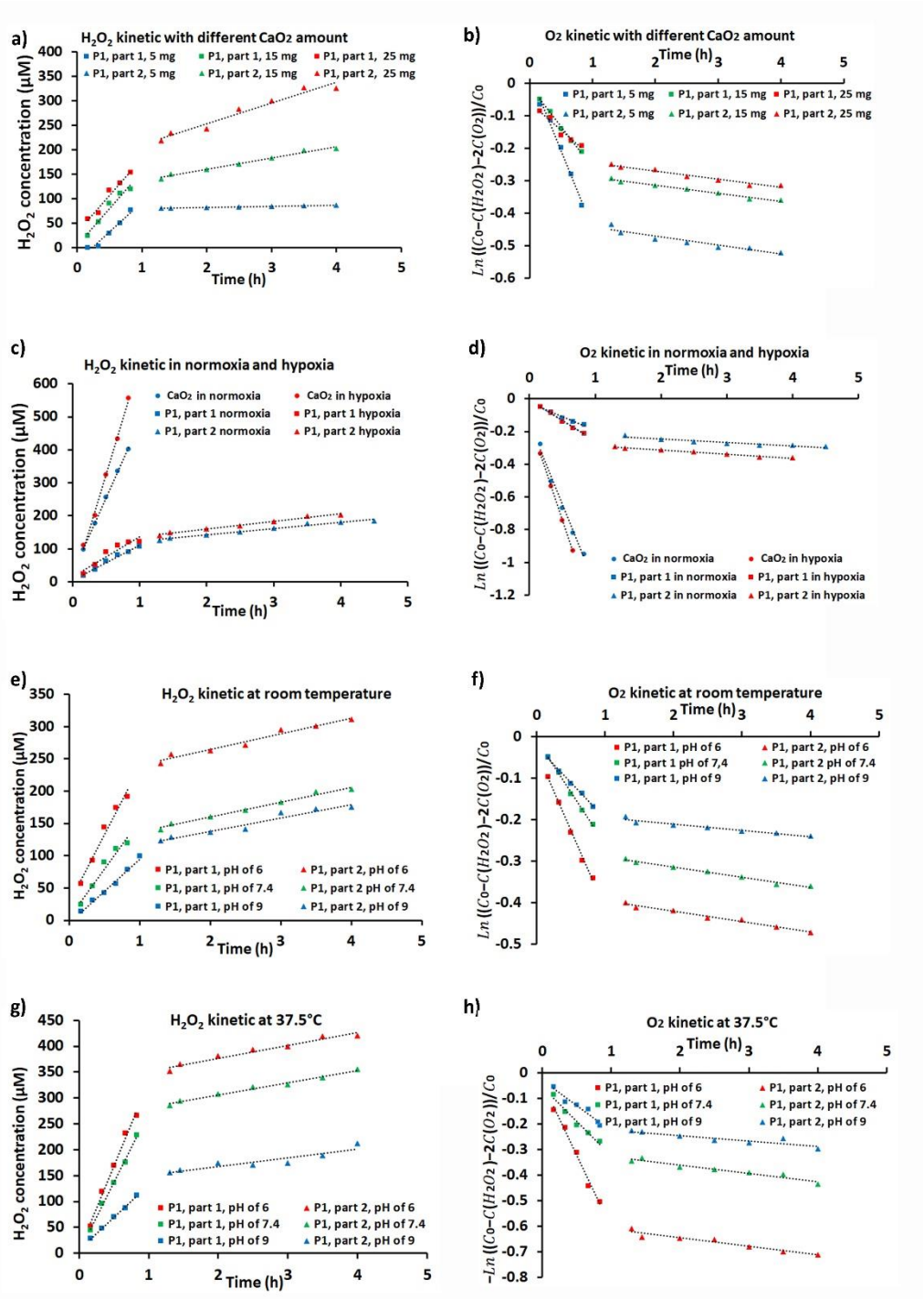

667

Figure 9. The kinetics of O_2 and H_2O_2 (a and b) of 5, 15, 25 mg of CaO_2 and a certain amount of P1 particles containing 5, 15, 25 mg of CaO_2, (c and d) of CaO_2 and P1 particles in hypoxia and normoxia (e and f), of P1 particles in hypoxia and different pHs at room temperature, and (g and h) of P1 particles in hypoxia and different pHs at 37 °C.

3.5 Release and kinetic of O_2 and H_2O_2 from films containing the particles

The challenge associated with utilizing O_2-generating biomaterials lies in the toxic burst release. Despite the efforts to extend the release rate by encapsulating the biomaterials within hydrophobic shells, these shells are unable to mitigate the initial burst release[7]. While the PCL shell could sustain an O_2 supply for up to 96 hours, the release rate was still rapid. To address this issue, the P1 particles were incorporated into PFC-chitosan films, facilitating the controlled release of generated O_2 through the PFC groups.

Figure 10a-d and Table 6 present the release and kinetics of O_2 and H_2O_2 from P1 particles and films. Given that CaO_2 might partially decompose during the film synthesis process since the PFC chitosan was dissolved in a mix of THF and water, an excessive amount of P1 particles were added to the films to compensate for the decomposed amount of CaO_2. Knowing that the synthesis takes 1 hour, we calculated the decomposed amount of CaO_2 by converting the concentrations of O_2 and H_2O_2 that can be released during this time to the gram of CaO_2. This calculated amount of P1 was then incorporated into the PFC-chitosan films.

Incorporating P1 into the PFC-chitosan film acted as a second barrier and reduced the yield of O_2 and H_2O_2 (Figures 10a and b). The impact of PFC-chitosan films on the release of O_2 was more intense than H_2O_2 since the change in k_{O_2} of P1F0.5 and P1F1 was higher than the change in $k_{H_2O_2}$ of P1F0.5 and P1F1 when compare to k_{O_2} and $k_{H_2O_2}$ of P1 (Table 6). By increasing the PFC-chitosan the k_{O_2} decreased (Table 6). Therefore, incorporating the particles into the PFC-chitosan films could decrease the initial burst release of O_2.

In contrast, PFC-chitosan films did not affect on kinetic of H_2O_2. Therefore, it can be concluded that PFC groups could dissolve the generated O_2 and release the dissolved O_2 in a controlled manner due to the weak intermolecular forces (van der Waals interactions) between O_2 molecules and PFC groups (Figure 10c and d)[59].

The k_{O_2} of P1F0.5 and P1F1 in part 2 were higher than k_{O_2} of P1 that showed PFCs groups supplied the generated O_2 in part 1 with a sustained rate in part 2. The change in the k_{O_2} and $k_{H_2O_2}$ at the termination of the CaO_2 was observed even with incorporating P1 into the PFC-chitosan film. Similar to the particles, it was assumed that covered CaO_2 in the outer layer of PCL with more possibility of exposure to water changed the rate of the releases. Partially encapsulated CaO_2 was detected on the surface of the films (Figure 4a).

The conjugated PFCs groups on different polymers have been utilized as O_2-carrying materials[23, 60, 61]. Fluorinated methacrylamide chitosan (MACF) hydrogels were synthesized by Patil et al. to deliver O_2 for enhancing collagen synthesis in wound healing[30]. Since the MACF hydrogels had not self an O_2-generating ability, the hydrogels were needed to saturated by O_2. It was reported that the saturated hydrogels increased the partial pressure of O_2 from 159 mmHg, which is the atmospheric O_2 tension, to 265 mmHg in 1 hour. After 2 days the partial pressure of O_2 decreased to 169 mmHg.

Moreover, Wijekoon et al synthesized MACF hydrogels with different types of fluorine groups to design adaptable O_2 carriers [23]. All the designed hydrogels required to be saturated and could supply O_2 for up to 14 hours. While our PFC-chitosan can generate O_2 in situ without needing to be saturated by pure O_2 and provide O_2.

Table 6. k_{O_2} and $k_{H_2O_2}$ of the generated O_2 and H_2O_2 from P1, P1F0.5, and P1F1.

Samples	k_{O_2} ($\mu M^{-1} h^{-1}$)		$k_{H_2O_2}$ ($\mu M^{-1} h^{-1}$)	
	Part 1	Part 2	Part 1	Part 2
P1	0.249	0.028	149.650	25.572
P1F1	0.146	0.044	119.740	31.082
P1F0.5	0.141	0.037	137.570	24.157

3.6 O_2 preservation of the particles and films

Given that the k_{O_2} of the films was higher than the k_{O_2} of CaO_2 and P1 (Table 4 and Table 6), it was hypothesized that the films could sustainably release dissolved O_2 by PFCs groups. The preservation ability of O_2 in the films and particles was studied by adding a certain amount of samples containing 15 mg of CaO_2 in 100 mL of unsealed release media at room temperature and a pH of 7.4, in normoxia.

The concentration of O_2 generated from CaO_2 exhibited a reduction from 456.63 μM to 209.13 μM within less than 24 hours (Figure 10e). However, P1 demonstrated the capability to generate O_2 for 96 hours (Figure 8c) and thereby exhibited a higher concentration of O_2 than CaO_2. The introduction of PFC groups onto chitosan resulted in an improved ability to preserve O_2, as evidenced by the final concentration of O_2 after 268 hours for P1F1 being 26.32 μM higher than that of P1. Moreover, the augmentation of PFCs content in PFC-chitosan films further improved the ability to preserve the generated O_2 in comparison to P1, as demonstrated by P1F0.5 (Figure 10e). The incorporation of O_2-generating particles into PFC-chitosan facilitated the binding of O_2, thereby leading to an augmentation of O_2 preservation.

Therefore, the utilization of PFC-chitosan films not only exhibited the ability to decelerate the initial burst release of O_2 from P1 particles but also extended the supply of O_2 in the release media. The O_2-preserving capability of PFC groups has been leveraged extensively in delivering O_2 to wound sites. For example, Niu et al. developed hydrogels with a high capacity for preserving O_2, wherein the hydrogels with PFC groups exhibited a significantly higher concentration of O_2 after 168 hours, in contrast to those without such groups[62].

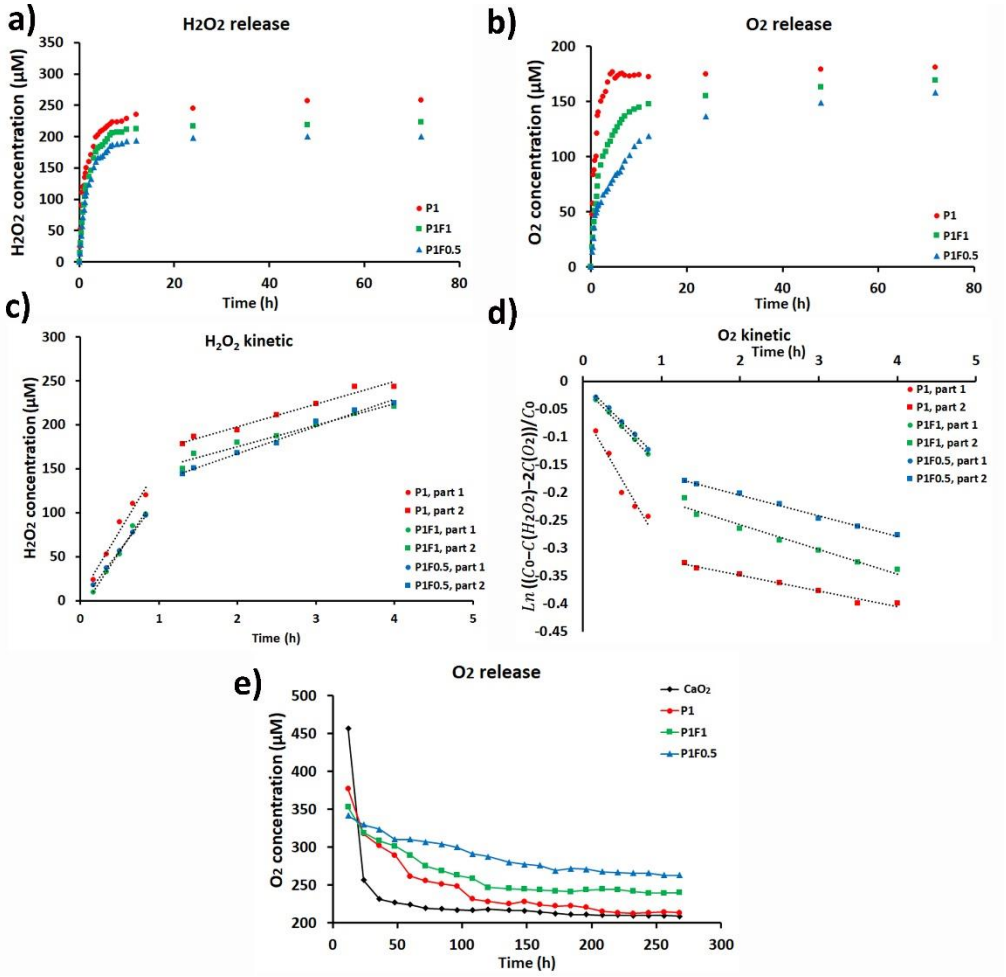

Figure 10. (a and b) H_2O_2 and O_2 release from P1, P1F0.5, and P1F1, (c and d) the kinetics of H_2O_2 and O_2 from P1, P1F0.5, and P1F1, and (e) O_2 preserving of CaO_2, P1, P1F0.5, and P1F1 at pH of 7.4 and the room temperature in 100 mL of the release media with normoxia condition.

3.7 The potential of the films to provide O_2 for wound healing

The requirement for O_2 concentration and its role in each phase of wound healing differs[63]. Studies have estimated that wound O_2 tension varies in different parts of the wound during the inflammatory phase, with values ranging from 0-10 mmHg in the center, 60 mmHg at the periphery, and 100 mmHg in the arteries[63]. It has also been noted that fibroblasts responsible for depositing collagen require an O_2 tension of 30-40 mmHg[63]. To ensure optimal wound healing, wound dressings must provide the necessary concentration of O_2. A study by Zhang et al. presents the development of Gelatin Methacryloyl (GelMA) based microneedles containing hemoglobin as a means of delivering O_2 to the wound site[64]. The microneedles were able to

generate approximately 45 mmHg of O_2 in PBS buffer in the presence of a near-infrared ray (NIR). It has been demonstrated that microneedles are effective in treating wounds in a type I diabetes rat model[64].

P1 particles containing 15 mg of the loaded CaO_2 were able to generate a constant amount of 179.01±13.50 µM of O_2 (Table 3). Assuming a constant temperature (room temperature) and constant pressure (1008 mbar), this O_2 release equates to 107.03±11.50 mmHg. Thus, the necessary quantity of particles can be calculated based on the wound stage and the required O_2 pressure to provide the necessary O_2 pressure for wound healing.

In the present work, the PCL particles extended the termination time of CaO_2 decomposition from 50 minutes to 96 hours. Other methods of incorporating CaO_2 into PCL, such as W/O emulsion, single nozzle electrospray, and co-axial nozzle electrospray, have been reported to provide O_2 release for periods ranging from 96 hours to 144 hours. The synthesized particles increased the dissolved O_2 tension to approximately 25-35% on the first day, with the concentration decreasing over time (low O_2 preservation)[20]. The electrospray synthesis of PCL particles containing CaO_2 by Morais et al. resulted in a 168-hour release of O_2, with the maximum concentration observed at the end of the first day[38].

3.8 In vitro assays

The results indicated that particles and films containing CaO_2 without catalase showed significantly higher ROS production compared to the control and samples containing CaO_2 in the presence of catalase (Figure 11). These findings suggest that the generated H_2O_2 from CaO_2 decomposition has the potential to induce oxidative stress and cellular damage. However, the presence of catalase in the cell media allowed the generated H_2O_2 to decompose to water and O_2, without showing ROS production. Additionally, the P1 particle with the higher H_2O_2 release rate had a higher ROS production compared to P1F0.5 and P1F1 films.

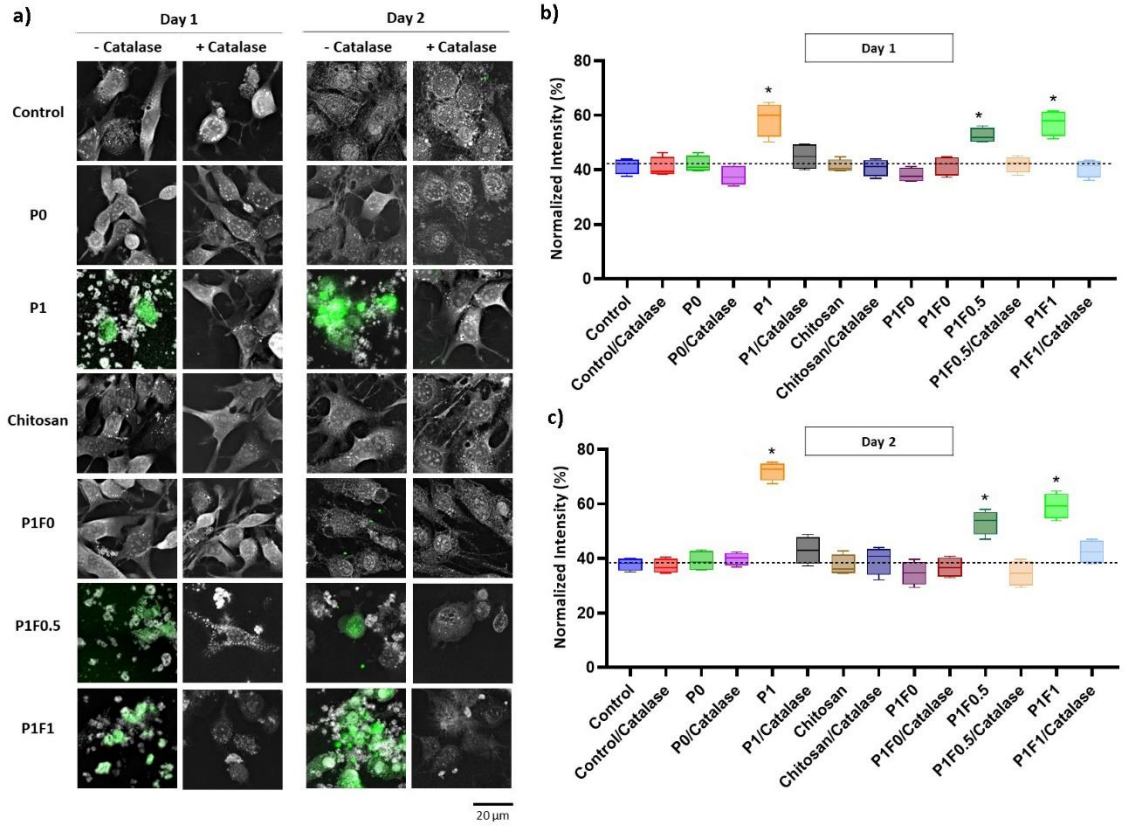

Figure 11. (a) ROS generation in Fibroblast cells before (control) and after treatment by P0, P1, chitosan, P1F0, P1F0.5, and P1F1 with and without catalase, (b) the normalized value of the green intensity from control, P0, P1, chitosan, P1F0, P1F0.5, and P1F1 with and without catalase after 1-day incubation, and (c) the normalized value of the green intensity from control, P0, P1, chitosan, P1F0, P1F0.5, and P1F1 with and without catalase after 2 days incubation.

Cell viability of the samples was studied in normoxia and hypoxia to investigate the effect of the generated O_2 and H_2O_2 as well as modification of chitosan by PFC groups and loading CaO_2 into PCL particles on the cell viability. The particles and films containing CaO_2 without catalase had significant cell toxicity in both hypoxia and normoxia (Figure 12) due to the oxidative stress caused by the H_2O_2 generated from the CaO_2 decomposition, as indicated by the ROS generation results (Figure 11). However, the use of catalase to decompose H_2O_2 into O_2 and water alleviated the cell toxicity of particles and films containing O_2-generating sources.

In normoxia, P1 particles with catalase showed lower cell viability than the control, P1F0.5, and P1F1 with catalase at days 2 and 4 due to the high O_2 generation rate from P1. However,

P1F0.5 and P1F1 had the same cell viability as the control due to their lower O_2 release compared to P1/catalase.

The particles and films containing CaO_2 could alleviate hypoxia and increase cell viability in the presence of catalase. Moreover, the comparison of cell viability of chitosan and P1F0 in hypoxia and normoxia showed that the modification of chitosan with PFCs groups did not have a toxic effect. Additionally, the comparison between the cell viability of P0 and P1 revealed that the observed toxicity in P1 was due to CaO_2.

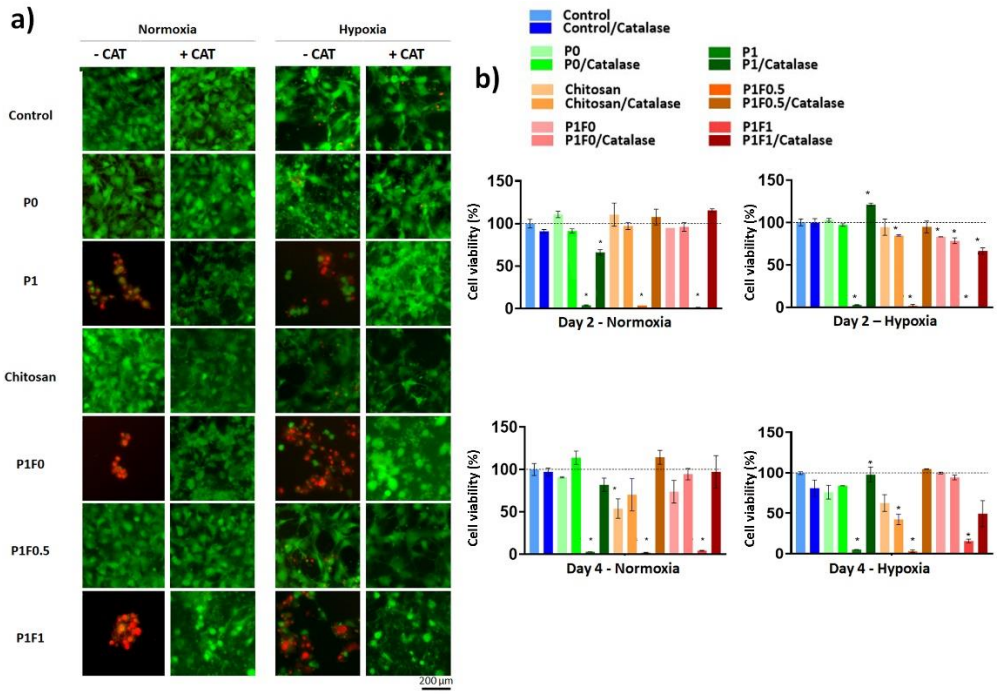

Figure 12. (a) Live/Dead^{TM} and (b) cell viability of P0, P1, chitosan, P1F0, P1F0.5, and P1F1 with and without catalase.

Increasing the supply of O_2 has been shown to have positive effects on promoting angiogenesis and epithelialization and reducing inflammation. Thus, the potential of P1F1 films to generate simultaneous H_2O_2 and O_2 for treating vascular disorders was investigated using the CAM assay. The total length (% mm mm^{-1}) and number of blood vessel junctions around P1F1 and P1F0 significantly increased over time, from 0 to 48 hours after incubation (Figure 13). Notably, the total length and number of junctions in P1F1 at 24 and 48 hours were higher than those of P1F0 and the control, indicating that the simultaneous generation of O_2 and H_2O_2 improved angiogenesis in the CAM assay. These results correspond well with previous findings

demonstrating that acute oxidative stress and O_2 can stimulate the surrounding tissues, resulting in increased recruitment of blood vessels and neovascularization [65-67].

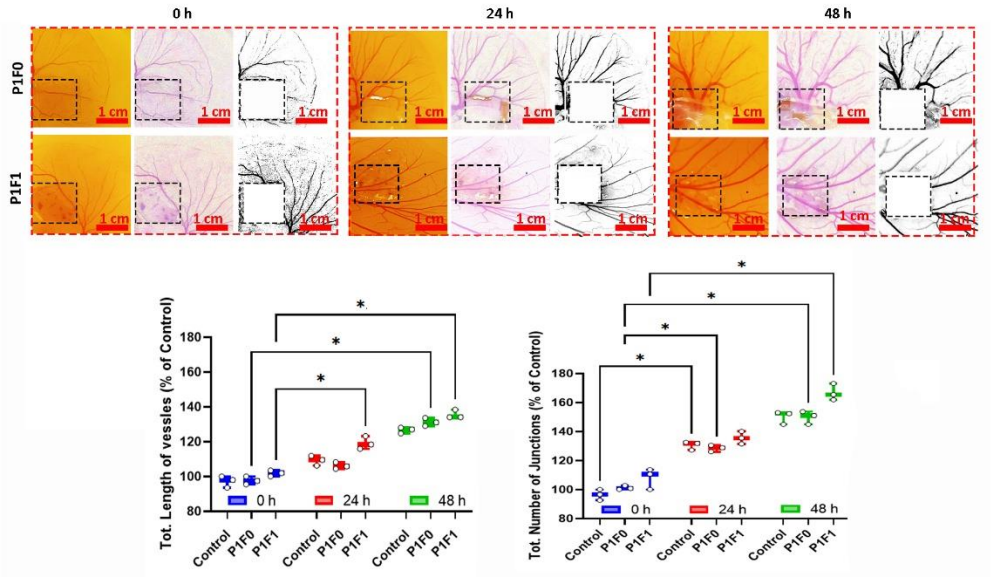

Figure 13. Investigation of the angiogenic properties of the films in CAM assay. The films were placed on vessels junction and marked with a black rectangle. The first column in each time point (0, 24, and 48 h) demonstrates chicken egg embryos incubated with P1F0 and P1F1 films for 0, 24, and 48 hours. The second and third columns show the images of the incubated chicken egg embryos with the films used for vessel length (% mm mm^{-1}) and junctions numbers analysis by Angiogenesis Analyzer in ImageJ®. As well as the total length and the total number of junctions of blood vessels around the samples have been quantified.

4. Conclusion

Incorporating CaO_2 into hydrophobic shells can prevent CaO_2 decomposition and extend the release time of O_2. Embedding the particles, which contain CaO_2, into PFC-chitosan films can effectively slow down the initial burst release and enhance the preservation time of O_2 in the release media. This is due to an increase in O_2 solubility in water brought about by the presence of PFC groups.

The kinetic studies on O_2 and H_2O_2 releasing of loaded CaO_2 in PCL particles and the particles embedded in PFC-chitosan films under various conditions showed that the kinetics of O_2 releasing of either the particles or the particles embedded in the film was different. The O_2-suppling time of the particles is shorter than that of the film. Furthermore, the O_2-releasing rates of the

particles are quicker than those of PFC-chitosan films as well. The O_2 and H_2O_2 release kinetics were affected by pH, temperature, and the concentration of initial CaO_2 and O_2 of the media (driving force). The release of H_2O_2 and O_2 was pH-dependent, and at basic pH, O_2 generation was dominant. However, we acknowledge that our study has certain limitations, including the need for further investigations to elucidate the exact mechanisms governing gas release, particularly the role of both larger and nanoscale pores observed in the PCL particles.

The particles and films containing CaO_2 showed oxidative stress without catalase and in the presence of catalase no oxidative stress was observed. The particles with higher O_2 releasing rate than films have less cell viability on normoxia. The simultaneous generation of O_2 and H_2O_2 improved the angiogenesis in CAM assay.

Acknowledgments

This research work was supported by Aspirant fellowships from the Fonds National de la Recherche Scientific de Belgique (FNRS) (grant number 38351, 2021 awarded to Pejman Ghaffari-Bohlouli).

Conflict of Interest

The authors declare no conflict of interest.

Data Availability Statement

The data that support the findings of this study are available from the corresponding author upon reasonable request.

References

[1] M.J. Malone-Povolny, S.E. Maloney, M.H. Schoenfisch, Nitric oxide therapy for diabetic wound healing, Advanced healthcare materials 8(12) (2019) 1801210.
[2] S.-B. Catrina, X. Zheng, Hypoxia and hypoxia-inducible factors in diabetes and its complications, Diabetologia 64(4) (2021) 709-716.
[3] N.G. Willemen, S. Hassan, M. Gurian, J. Li, I.E. Allijn, S.R. Shin, J. Leijten, Oxygen-releasing biomaterials: current challenges and future applications, Trends in biotechnology 39(11) (2021) 1144-1159.
[4] S. Sen, S. Sen, Therapeutic effects of hyperbaric oxygen: integrated review, Medical Gas Research 11(1) (2021) 30.
[5] S.E. Salama, A.E. Eldeeb, A.H. Elbarbary, S.E. Abdelghany, Adjuvant hyperbaric oxygen therapy enhances healing of nonischemic diabetic foot ulcers compared with standard wound care alone, The international journal of lower extremity wounds 18(1) (2019) 75-80.

[6] Y. Qiao, F. Yang, T. Xie, Z. Du, D. Zhong, Y. Qi, Y. Li, W. Li, Z. Lu, J. Rao, Engineered algae: A novel oxygen-generating system for effective treatment of hypoxic cancer, Science Advances 6(21) (2020) eaba5996.
[7] N. Ashammakhi, M.A. Darabi, N.S. Kehr, A. Erdem, S.-k. Hu, M.R. Dokmeci, A.S. Nasr, A. Khademhosseini, Advances in controlled oxygen generating biomaterials for tissue engineering and regenerative therapy, Biomacromolecules 21(1) (2019) 56-72.
[8] P. Chairuangkitti, S. Lawanprasert, S. Roytrakul, S. Aueviriyavit, D. Phummiratch, K. Kulthong, P. Chanvorachote, R. Maniratanachote, Silver nanoparticles induce toxicity in A549 cells via ROS-dependent and ROS-independent pathways, Toxicology in vitro 27(1) (2013) 330-338.
[9] C.I. Castro, J.C. Briceno, Perfluorocarbon-based oxygen carriers: review of products and trials, Artificial organs 34(8) (2010) 622-634.
[10] P.S. Patil, S. Fathollahipour, A. Inmann, A. Pant, R. Amini, L.P. Shriver, N.D. Leipzig, Fluorinated methacrylamide chitosan hydrogel dressings improve regenerated wound tissue quality in diabetic wound healing, Advances in Wound Care 8(8) (2019) 374-385.
[11] E. Mohseni-Vadeghani, R. Karimi-Soflou, S. Khorshidi, A. Karkhaneh, Fabrication of oxygen and calcium releasing microcarriers with different internal structures for bone tissue engineering: Solid filled versus hollow microparticles, Colloids and Surfaces B: Biointerfaces 197 (2021) 111376.
[12] Z. Zhang, Z. Rong, G. Wu, Y. Wang, Z. Tan, J. Zheng, Y. Jin, Z. Liang, C. Liu, J. Guo, Gelatin-CaO2/SAP/PLGA composite scaffold enhances the reparation of critical-sized cranial defects by promoting seed cell survival, Applied Materials Today 22 (2021) 100960.
[13] E.M. Lee, J.I. Jung, Z. Alam, H.G. Yi, H. Kim, J.W. Choi, S. Hurh, Y.J. Kim, J.C. Jeong, J. Yang, Effect of an oxygen-generating scaffold on the viability and insulin secretion function of porcine neonatal pancreatic cell clusters, Xenotransplantation 25(2) (2018) e12378.
[14] T. Zou, S. Jiang, Y. Zhang, J. Liu, B. Yi, Y. Qi, W. Dissanayaka, C. Zhang, In situ oxygen generation enhances the SCAP survival in hydrogel constructs, Journal of dental research 100(10) (2021) 1127-1135.
[15] K. Joshi Navare, T. Colombani, M. Rezaeeyazdi, N. Bassous, D. Rana, T. Webster, A. Memic, S.A. Bencherif, Needle-injectable microcomposite cryogel scaffolds with antimicrobial properties, Scientific Reports 10(1) (2020) 1-16.
[16] G. Qian, J. Wang, L. Yang, Z. Zeng, Z. Zhao, S. Peng, C. Shuai, A pH-responsive CaO2@ ZIF-67 system endows a scaffold with chemodynamic therapy properties, Journal of Materials Science (2023) 1-15.
[17] P. Mostafalu, A. Tamayol, R. Rahimi, M. Ochoa, A. Khalilpour, G. Kiaee, I.K. Yazdi, S. Bagherifard, M.R. Dokmeci, B. Ziaie, Smart bandage for monitoring and treatment of chronic wounds, Small 14(33) (2018) 1703509.
[18] K. Maliyar, R. Persaud-Jaimangal, R.G. Sibbald, Associations among skin surface pH, temperature, and bacterial burden in wounds, Advances in Skin & Wound Care 33(4) (2020) 180-185.
[19] H. Wang, Y. Zhao, T. Li, Z. Chen, Y. Wang, C. Qin, Properties of calcium peroxide for release of hydrogen peroxide and oxygen: a kinetics study, Chemical Engineering Journal 303 (2016) 450-457.
[20] M. Zhang, T. Kiratiwongwan, W. Shen, Oxygen-releasing polycaprolactone/calcium peroxide composite microspheres, Journal of Biomedical Materials Research Part B: Applied Biomaterials 108(3) (2020) 1097-1106.
[21] S. Suvarnapathaki, M.A. Nguyen, A.A. Goulopoulos, D. Lantigua, G. Camci-Unal, Engineering calcium peroxide based oxygen generating scaffolds for tissue survival, Biomaterials Science 9(7) (2021) 2519-2532.
[22] Z.E. Cele, A.M. Somboro, D.G. Amoako, L.F. Ndlandla, M.O. Balogun, Fluorinated quaternary chitosan derivatives: Synthesis, characterization, antibacterial activity, and killing kinetics, ACS omega 5(46) (2020) 29657-29666.
[23] A. Wijekoon, N. Fountas-Davis, N.D. Leipzig, Fluorinated methacrylamide chitosan hydrogel systems as adaptable oxygen carriers for wound healing, Acta biomaterialia 9(3) (2013) 5653-5664.

[24] P.S. Patil, M.M. Evancho-Chapman, H. Li, H. Huang, R.L. George, L.P. Shriver, N.D. Leipzig, Fluorinated methacrylamide chitosan hydrogel dressings enhance healing in an acute porcine wound model, PloS one 13(9) (2018) e0203371.
[25] P. Le Thi, Y. Lee, D.L. Tran, T.T.H. Thi, K.M. Park, K.D. Park, Calcium peroxide-mediated in situ formation of multifunctional hydrogels with enhanced mesenchymal stem cell behaviors and antibacterial properties, Journal of Materials Chemistry B 8(48) (2020) 11033-11043.
[26] S. Park, K.M. Park, Hyperbaric oxygen-generating hydrogels, Biomaterials 182 (2018) 234-244.
[27] R.L. da Silva, O.D. Bernardinelli, E.C. Frachini, H. Ulrich, E. Sabadini, D.F. Petri, Vanillin crosslinked chitosan films: The states of water and the effect of carriers on curcumin uptake, Carbohydrate Polymers 292 (2022) 119725.
[28] A.A. Shitole, P.W. Raut, N. Sharma, P. Giram, A.P. Khandwekar, B. Garnaik, Electrospun polycaprolactone/hydroxyapatite/ZnO nanofibers as potential biomaterials for bone tissue regeneration, Journal of Materials Science: Materials in Medicine 30 (2019) 1-17.
[29] P. Ghaffari-Bohlouli, M. Shahrousvand, P. Zahedi, M. Shahrousvand, Performance evaluation of poly (L-lactide-co-D, L-lactide)/poly (acrylic acid) blends and their nanofibers for tissue engineering applications, International journal of biological macromolecules 122 (2019) 1008-1016.
[30] P.S. Patil, N. Fountas-Davis, H. Huang, M.M. Evancho-Chapman, J.A. Fulton, L.P. Shriver, N.D. Leipzig, Fluorinated methacrylamide chitosan hydrogels enhance collagen synthesis in wound healing through increased oxygen availability, Acta biomaterialia 36 (2016) 164-174.
[31] S. Moghassemi, A. Dadashzadeh, P.E.N. de Souza, R.B. Azevedo, C.A. Amorim, AlPc/ZnPc-based oncological photodynamic therapy for a selective eradication of leukemic cells from ovarian tissue, Photodiagnosis and photodynamic therapy 36 (2021) 102555.
[32] S. Moghassemi, A. Dadashzadeh, A. Camboni, O. Feron, R.B. Azevedo, C.A. Amorim, Photodynamic therapy using OR141-loaded nanovesicles for eradication of leukemic cells from ovarian tissue, Photodiagnosis and photodynamic therapy 40 (2022) 103139.
[33] C.A. Schneider, W.S. Rasband, K.W. Eliceiri, NIH Image to ImageJ: 25 years of image analysis, Nature methods 9(7) (2012) 671-675.
[34] N.i. Mangir, S. Dikici, F. Claeyssens, S. MacNeil, Using ex ovo chick chorioallantoic membrane (CAM) assay to evaluate the biocompatibility and angiogenic response to biomaterials, ACS Biomaterials Science & Engineering 5(7) (2019) 3190-3200.
[35] L. Faihs, B. Firouz, P. Slezak, C. Slezak, M. Weißensteiner, T. Ebner, N. Ghaffari Tabrizi-Wizsy, K. Schicho, P. Dungel, A Novel Artificial Intelligence-Based Approach for Quantitative Assessment of Angiogenesis in the Ex Ovo CAM Model, Cancers 14(17) (2022) 4273.
[36] J. Simińska-Stanny, F. Hachemi, G. Dodi, F.D. Cojocaru, I. Gardikiotis, D. Podstawczyk, C. Delporte, G. Jiang, L. Nie, A. Shavandi, Optimizing phenol-modified hyaluronic acid for designing shape-maintaining biofabricated hydrogel scaffolds in soft tissue engineering, International journal of biological macromolecules (2023) 125201.
[37] R.B. Yoganathan, R. Mammucari, N.R. Foster, A green method for processing polymers using dense gas technology, Materials 3(5) (2010) 3188-3203.
[38] A.I. Morais, X. Wang, E.G. Vieira, B.C. Viana, E.C. Silva-Filho, J.A. Osajima, S. Afewerki, M.A. Corat, H.S. Silva, F.R. Marciano, Electrospraying oxygen-generating microparticles for tissue engineering applications, International Journal of Nanomedicine 15 (2020) 1173.
[39] K.M. Gattás-Asfura, C.A. Fraker, C.L. Stabler, Perfluorinated alginate for cellular encapsulation, Journal of biomedical materials research Part A 100(8) (2012) 1963-1971.
[40] G. Lawrie, I. Keen, B. Drew, A. Chandler-Temple, L. Rintoul, P. Fredericks, L. Grøndahl, Interactions between alginate and chitosan biopolymers characterized using FTIR and XPS, Biomacromolecules 8(8) (2007) 2533-2541.

[41] M.F. Queiroz, K.R. Teodosio Melo, D.A. Sabry, G.L. Sassaki, H.A.O. Rocha, Does the use of chitosan contribute to oxalate kidney stone formation?, Marine drugs 13(1) (2014) 141-158.
[42] Y. Xing, X. Li, X. Guo, W. Li, J. Chen, Q. Liu, Q. Xu, Q. Wang, H. Yang, Y. Shui, Effects of different TiO2 nanoparticles concentrations on the physical and antibacterial activities of chitosan-based coating film, Nanomaterials 10(7) (2020) 1365.
[43] J.R. Parsons, M. Sáez, J. Dolfing, P. De Voogt, Biodegradation of perfluorinated compounds, Reviews of Environmental Contamination and Toxicology Vol 196 (2008) 53-71.
[44] V. Jovicic, M.J. Khan, A. Zbogar-Rasic, N. Fedorova, A. Poser, P. Swoboda, A. Delgado, Degradation of low concentrated perfluorinated compounds (PFCS) from water samples using non-thermal atmospheric plasma (NTAP), Energies 11(5) (2018) 1290.
[45] D. Wu, Z.-Q. Zhu, H.-X. Tang, Z.-E. Shi, J. Kang, Q. Liu, J. Qi, Efficacy-shaping nanomedicine by loading calcium peroxide into tumor microenvironment-responsive nanoparticles for the antitumor therapy of prostate cancer, Theranostics 10(21) (2020) 9808.
[46] T.-E. Hsieh, S.-J. Lin, L.-C. Chen, C.-C. Chen, P.-L. Lai, C.-C. Huang, Optimizing an injectable composite oxygen-generating system for relieving tissue hypoxia, Frontiers in Bioengineering and Biotechnology 8 (2020) 511.
[47] C. Liu, Y. Cao, Y. Cheng, D. Wang, T. Xu, L. Su, X. Zhang, H. Dong, An open source and reduce expenditure ROS generation strategy for chemodynamic/photodynamic synergistic therapy, Nature communications 11(1) (2020) 1735.
[48] Q. Sun, B. Liu, R. Zhao, L. Feng, Z. Wang, S. Dong, Y. Dong, S. Gai, H. Ding, P. Yang, Calcium peroxide-based nanosystem with cancer microenvironment-activated capabilities for imaging guided combination therapy via mitochondrial Ca2+ overload and chemotherapy, ACS Applied Materials & Interfaces 13(37) (2021) 44096-44107.
[49] A. Rastinfard, M.H. Nazarpak, F. Moztarzadeh, Controlled chemical synthesis of CaO 2 particles coated with polyethylene glycol: Characterization of crystallite size and oxygen release kinetics, RSC advances 8(1) (2018) 91-101.
[50] A.J. Waite, J.S. Bonner, R. Autenrieth, Kinetics and stoichiometry of oxygen release from solid peroxides, Environmental engineering science 16(3) (1999) 187-199.
[51] T. Colombani, L.J. Eggermont, S.M. Hatfield, Z.J. Rogers, M. Rezaeeyazdi, A. Memic, M.V. Sitkovsky, S.A. Bencherif, Oxygen-Generating Cryogels Restore T Cell Mediated Cytotoxicity in Hypoxic Tumors, Advanced Functional Materials 31(37) (2021) 2102234.
[52] A.I. Morais, X. Wang, E.G. Vieira, B.C. Viana, E.C. Silva-Filho, J.A. Osajima, S. Afewerki, M.A. Corat, H.S. Silva, F.R. Marciano, Electrospraying oxygen-generating microparticles for tissue engineering applications, International Journal of Nanomedicine (2020) 1173-1186.
[53] I. Arany, J.K. Megyesi, H. Kaneto, S. Tanaka, R.L. Safirstein, Activation of ERK or inhibition of JNK ameliorates H2O2 cytotoxicity in mouse renal proximal tubule cells, Kidney international 65(4) (2004) 1231-1239.
[54] H. Zhang, J.E. Barralet, Mimicking oxygen delivery and waste removal functions of blood, Advanced Drug Delivery Reviews 122 (2017) 84-104.
[55] G. Nindl, N.R. Peterson, E.F. Hughes, L.R. Waite, M.T. Johnson, Effect of hydrogen peroxide on proliferation, apoptosis and interleukin-2 production of Jurkat T cells, Biomedical sciences instrumentation 40 (2004) 123-128.
[56] M. Bagatini, C. Assmann, M. Blumenberg, Glutathione System and Oxidative Stress in Health and Disease, BoD–Books on Demand2020.
[57] P. Pędziwiatr, Decomposition of hydrogen peroxide-kinetics and review of chosen catalysts, Acta Innovations (26) (2018) 45-52.

[58] R. Derwin, D. Patton, P. Avsar, H. Strapp, Z. Moore, The impact of topical agents and dressing on pH and temperature on wound healing: A systematic, narrative review, International Wound Journal 19(6) (2022) 1397-1408.
[59] J.G. Riess, Understanding the fundamentals of perfluorocarbons and perfluorocarbon emulsions relevant to in vivo oxygen delivery, Artificial cells, blood substitutes, and biotechnology 33(1) (2005) 47-63.
[60] G. Li, S. Wang, D. Deng, Z. Xiao, Z. Dong, Z. Wang, Q. Lei, S. Gao, G. Huang, E. Zhang, Fluorinated chitosan to enhance transmucosal delivery of sonosensitizer-conjugated catalase for sonodynamic bladder cancer treatment post-intravesical instillation, ACS nano 14(2) (2020) 1586-1599.
[61] T. Zhu, L. Shi, C. Ma, L. Xu, J. Yang, G. Zhou, X. Zhu, L. Shen, Fluorinated chitosan-mediated intracellular catalase delivery for enhanced photodynamic therapy of oral cancer, Biomaterials Science 9(3) (2021) 658-662.
[62] H. Niu, C. Li, Y. Guan, Y. Dang, X. Li, Z. Fan, J. Shen, L. Ma, J. Guan, High oxygen preservation hydrogels to augment cell survival under hypoxic condition, Acta biomaterialia 105 (2020) 56-67.
[63] P.G. Rodriguez, F.N. Felix, D.T. Woodley, E.K. Shim, The role of oxygen in wound healing: a review of the literature, Dermatologic surgery 34(9) (2008) 1159-1169.
[64] X. Zhang, G. Chen, Y. Liu, L. Sun, L. Sun, Y. Zhao, Black phosphorus-loaded separable microneedles as responsive oxygen delivery carriers for wound healing, ACS nano 14(5) (2020) 5901-5908.
[65] Y. Lee, J.Y. Son, J.I. Kang, K.M. Park, K.D. Park, Hydrogen peroxide–releasing hydrogels for enhanced endothelial cell activities and neovascularization, ACS applied materials & interfaces 10(21) (2018) 18372-18379.
[66] M. Zehra, W. Zubairi, A. Hasan, H. Butt, A. Ramzan, M. Azam, A. Mehmood, M. Falahati, A.A. Chaudhry, I.U. Rehman, Oxygen generating polymeric nano fibers that stimulate angiogenesis and show efficient wound healing in a diabetic wound model, International journal of nanomedicine (2020) 3511-3522.
[67] Y. Guan, H. Niu, Z. Liu, Y. Dang, J. Shen, M. Zayed, L. Ma, J. Guan, Sustained oxygenation accelerates diabetic wound healing by promoting epithelialization and angiogenesis and decreasing inflammation, Science Advances 7(35) (2021) eabj0153.